Received: 24 April 2019 | Revised: 30 May 2019 | Accepted: 13 June 2019

DOI: 10.1002/aoc.5094

FULL PAPER

WILEY Applied Organometallic Chemistry

Polymer-anchored mononuclear and binuclear Cu^{II} Schiff-base complexes: Impact of heterogenization on liquid phase catalytic oxidation of a series of alkenes

Abhishek Maurya[1] | **Neha Kesharwani**[1] | **Payal Kachhap**[1] | **Vivek Kumar Mishra**[1] | **Nikita Chaudhary**[2] | **Chanchal Haldar**[1]

[1] Department of Chemistry, Indian Institute of Technology (Indian School of Mines), Dhanbad 826004Jharkhand, India

[2] Department of Chemistry and Polymer Science, Stellenbosch University, Matieland 7602Stellenbosch, South Africa

Correspondence
Chanchal Haldar, Department of Chemistry, Indian Institute of Technology (Indian School of Mines), Dhanbad 826004, Jharkhand, India.
Email: chanchal@iitism.ac.in

Funding information
Science and Engineering Research Board(SERB), Grant/Award Numbers: SB/EMEQ-055/2014 and SB/FT/CS-027/2014

Liquid phase catalytic oxidation of a number of alkenes, for example, cyclohexene, *cis*-cyclooctene, styrene, 1-methyl cyclohexene and 1-hexene, was performed using polymer-anchored copper (II) complexes PS-[Cu (sal-sch)Cl] (**5**), PS-[Cu (sal-tch)Cl] (**6**), PS-[CH_2{Cu (sal-sch)Cl}$_2$] (**7**) and PS-[CH_2{Cu (sal-tch) Cl}$_2$] (**8**). Neat complexes [Cu (sal-sch)Cl] (**1**), [Cu (sal-tch)Cl] (**2**), [CH_2{Cu (sal-sch)Cl}$_2$] (**3**) and [CH_2{Cu (sal-tch)Cl}$_2$] (**4**) were isolated by reacting $CuCl_2 \cdot 2H_2O$ with [Hsal-sch] (**I**), [Hsal-tch] (**II**), [H_2bissal-sch] (**III**) and [H_2bissal-tch] (**IV**), respectively, in refluxing methanol. Complexes **1–4** have been covalently anchored in Merrifield resin through the amine nitrogen of the semicarbazide or thiosemicarbazide moiety. A number of analytical, spectroscopic and thermal techniques, such as CHNS analysis, Fourier transform-infrared, UV–Vis, PMR, ^{13}C-NMR, electron paramagnetic resonance, scanning electron microscopy, energy-dispersive X-ray analysis, thermogravimetric analysis, atomic force microscopy, atomic absorption spectroscopy, and electrospray ionization-mass spectrometry, were used to analyze and establish the molecular structure of the ligands (**I**)–(**IV**) and complexes (**1**)–(**8**) in solid state as well as in solution state. Grafted complexes **5–8** were employed as active catalysts for the oxidation of a series of alkenes in the presence of hydrogen peroxide. Copper hydroperoxo species ([Cu^{III} (sal-sch)-O-O-H]), which is believed to be the active intermediate, generated during the catalytic oxidation of alkenes, are identified. It was found that supported catalysts are very economical, green and efficient in contrast to their neat complexes as well as most of the recently reported heterogeneous catalysts.

KEYWORDS

chloromethylated polystyrene, copper (II) complexes, electron paramagnetic resonance, heterogeneous catalysis, oxidation of alkenes

1 | INTRODUCTION

Conversion of alkenes into various oxygenated products is academically challenging and industrially important. There are mainly three processes, namely epoxidation, oxidative cleavage and allylic/benzylic oxidation,[1] by which unproductive alkenes can be transformed into synthetically and commercially important chemicals. Alkene

https://doi.org/10.1002/aoc.5094

epoxidation contributes important and vital epoxide intermediates for the synthesis of many pharmaceutical and fine chemicals.[2] Numerous chemicals, like alcohols, carbonyl compounds, glycols, alkanolamines and polymers, can be prepared from epoxides. Also, the epoxide ring can easily interact with a number of nucleophiles, hence epoxides are commonly used for the production of additives, anticorrosives, plasticizers, perfumes, epoxy resins and surfactants, etc.[3]

Besides epoxidation, oxidative cleavage of alkenes to the corresponding carbonyl compounds is another important reaction for the functionalization of olefins. In the preparation of important intermediates or stock chemicals, oxidative cleavage of alkenes appears to be a key process. For this oxidative cleavage, a large number of processes are documented in the literature. Classically, ozonolysis was a method for C=C bond cleavage in olefins.[1c] Because of the safety issues, usability of ozonolysis is often restricted.[4] A number of bibliographic evidence can be found where first-, second- or even third-row transition metals (e.g. Mn, Fe, Ru, Os, Au, Pd, W, Re, etc.)[5] were used to catalyze the oxidative cleavage of olefins in the absence of ozone. Despite the significant advancement in the field of oxidative cleavage of olefins, there is still a deficiency in economic and green catalytic processes.

Lastly, allylic oxidation of olefins and alkylarenes into corresponding carbonyl compounds and α,β-unsaturated enones through C-H bond activation is one of the important conversions with synthetic as well as industrial utility. Often allylic or benzylic oxidation processes of olefins and alkylarenes are connected with the preparation of drug precursors and are involved in the building blocks of many organic syntheses.[6] A number of organocatalysts have emerged in the field of allylic or benzylic oxidation, but the metal-based catalysts for this oxidation remain exceptionally efficient.[7]

Easy separation, recyclability, high thermal stability and the eco-friendly nature of heterogeneous catalysts make them an attractive alternative of homogeneous catalysts. Hence, heterogeneous catalysts are extensively used in the diverse field of catalysis. To make a sustainable and non-polluting catalytic cycle, covalently anchored homogeneous catalysts on to the surface of chloromethylated polystyrene crosslinked with divinyl benzene appear to be an exotic field of research in the area of oxidation of various organic substrates. Easy availability, simple functionalization process, elevated thermal stability and low price makes chloromethylated polystyrene an irresistible choice among various organic, inorganic and hybrid solid supports.

Herein we have reported four Cu^{II} complexes [Cu (sal-sch)Cl] (**1**), [Cu (sal-tch)Cl] (**2**), $[CH_2\{Cu\ (sal\text{-}sch)Cl\}_2]$ (**3**) and $[CH_2\{Cu\ (sal\text{-}tch)Cl\}_2]$ (**4**) synthesized by reacting $CuCl_2·2H_2O$ with [Hsal-sch] (**I**), [Hsal-tch] (**II**), $[H_2bissal\text{-}sch]$ (**III**) and $[H_2bissal\text{-}tch]$ (**IV**). Ligands **I** and **II** were prepared by reacting salicylaldehyde with semicarbazide hydrochloride and thiosemicarbazide, respectively, while ligands **III** and **IV** were synthesized by reacting 5,5′-methylenebis (2-hydroxybenzaldehyde) with semicarbazide hydrochloride and thiosemicarbazide, respectively. All the synthesized copper complexes were heterogenized by immobilizing on to the surface of chloromethylated polystyrene. The behavior of synthetic catalysts towards catalytic oxidation of various alkenes was closely monitored. The effect of solid support on alkenes oxidation was also examined. Based on UV–Vis spectroscopy, liquid chromatography-mass spectrometry (LC–MS) and electron paramagnetic resonance (EPR) analyses, catalytic cycle for the oxidation of alkenes by synthesized copper complexes in the presence of hydrogen peroxide was proposed.

2 | EXPERIMENTAL

2.1 | Materials

1,3,5-Trioxane (Sigma-Aldrich, USA), $CuCl_2·2H_2O$ (Loba-Chemie, India), salicylaldehyde (SRL, India), thiosemicarbazide (Avra, India), semicarbazide hydrochloride (Avra, India), Merrifield's peptide resin (3.5–4.5 mmol/g Cl^-, 1% crosslinked; Sigma-Aldrich, USA), potassium iodide (Rankem, India), cyclohexene (Alfa-Aesar, India), styrene (Alfa-Aesar, India), 1-methyl cyclohexene (Alfa-Aesar, India), *cis*-cyclooctene (Alfa-Aesar, India), 1-hexene (Alfa-Aesar, India), 30% H_2O_2 (Merck, India), 70% TBHP (Alfa-Aesar, India), Nujol (SRL, India), H_2SO_4 (Merck, India) and AR grade solvent (Merck & Rankem, India) were used as received. HPLC grade methanol (Spectrochem, India) was used for gas chromatography (GC) and GC–MS analysis. 5,5′-Methylenebis (*2*-hydroxybenzaldehyde) (H_2bissal) was prepared by following the reported method.[8]

2.2 | Physical methods and analysis

Fourier transform-infrared (FT-IR) spectra (4000–400 cm $^{-1}$) were recorded on Agilent Cary 600 Series FT-IR Spectrometer by ATR method. CHNS elemental analysis was done in CHNS elemental model electron probe microanalyser SX, CAMECA (France). The ^1H- and ^{13}C-NMR spectra of the ligands were recorded from Bruker AC-400 NMR spectrometer in dimethylsulfoxide (DMSO) solution using TMS as an internal standard. Electronic spectra of ligands and metal complexes were recorded in a SHIMADZU UV-1800 spectrophotometer using

DMF/methanol as a solvent, whereas electronic spectra of polymer-bound metal complexes were recorded by dispersing in Nujol (heavy paraffin wax). The presence of copper content and surface morphology of polymer-anchored copper complexes were analyzed by energy-dispersive X-ray analysis (EDX) and scanning electron microscopy (SEM) on a HITACHI S-3400 N instrument after coating the polymer bead surface with a thin film of gold to block the surface charging and thermal damage by the electron beam. A scanning probe microscope from DIMENSION iCON with ScanAsyst was used for atomic force microscopy (AFM) imaging. Thermogravimetric analysis (TGA) and differential thermal analysis (DTA) were performed by using Perkin Elmer, Diamond TG/DTA instrument. Copper content was confirmed by atomic absorption spectrometer (Model No. Lab India, AA 8000) after decomposing the polymer-anchored metal complexes by concentrate HNO_3 and subsequent dilution of the filtrate. The electrospray ionization $(ESI)^+$ mass of the metal complexes was estimated on Waters Q-Tof Micromass instrument. EPR spectra of the polymer-anchored metal complexes were recorded in a Bruker EMX X-band spectrometer operating at 100-kHz field modulation at room temperature. LC–MS analysis of the reactive intermediates was done on an Agilent (Model No. G1978 B) LC–MS instrument. The catalytic activity of various alkenes was monitored by an Agilent 7890 B GC fitted with an HP-5 capillary column (30 m × 0.25 mm × 0.25 μm), and an FID detector was used to analyze the reaction products. Oxidation products of various alkenes were identified by thermoscientific GC–MS (Model no. Trace 1300, ISQ QD) fitted with a TG-5MS capillary column (30 m × 0.25 mm × 0.25 μm) and an EI^+ mass detector.

2.3 | Density functional theory calculations

Gaussian '09 rev. D.01[9] was used to perform all the theoretical calculations. For the preparation of input files and visualization of the output files, GaussView 5.0.8[10] was used. Gas phase optimization of all ground state molecular structures was executed by density functional theory (DFT) in its unrestricted form using LANL2DZ with an effective core potential for Cu atoms and 6–311 + G(d, p) for the rest of the atoms (C, H, N, O, S and Cl), employing a HP-Z440 workstation. Becke3–Lee–Yang–Parr (B3LYP) procedure[11–13] was used to incorporate electron correlation into the DFT calculation. Initial geometry for the optimization was taken from single-crystal X-ray refinement data of the mononuclear [Cu (sal-sch)Cl](**1**).[14] Vibrational frequencies were calculated at the same level of theory. The absence of imaginary frequency signifies that optimized geometry appears for local minima. All the geometry optimizations were performed without any symmetry constrain.

2.4 | Synthesis of [Hsal-sch] (I) and [Hsal-tch] (II)

Ligand [Hsal-sch] (**I**) was prepared by the following method, which is different from the earlier reported method.[14] A methanolic solution (20 ml) of semicarbazide hydrochloride (1.1153 g, 10 mmol) was reacted with a methanolic solution (20 ml) of salicylaldehyde (1.2204 g, 10 mmol), and the resulting mixture was refluxed for ~4 hr (Scheme 1). The volume of the solution was reduced to ~10 ml and kept in a refrigerator where a white color solid separated out, which was filtered, washed with methanol and dried in vacuum over silica gel.

Data for [Hsal-sch] (**I**): yield: 70.45% (1.33 g); anal. calcd for $C_8H_9N_3O_2$ (MW 179.18); C, 53.63%; H, 5.06%; N, 23.45%. Found: C, 53.58%; H, 5.13%; N, 23.32%. FT-IR (ATR, cm^{-1}): 3479($\nu_{O\text{-}H}$), 3274($\nu_{N\text{-}H}$), 1684($\nu_{C=O}$), 1581($\nu_{C=N}$); UV–Vis [λ_{max} (nm), ε ($lmol^{-1}$ cm^{-1})]: 216 (2.07×10^3), 224 (sh), 277 (2.41×10^3), 286 (sh), 317 (1.48×10^3). ^{1}H-NMR (DMSO-d_6, δ in ppm): 6.24 (s, 2H), 6.75–6.79 (t, 1H), 6.80–6.82 (d, 1H), 7.09–7.13 (t, 1H), 7.52–7.53 (d, 1H), 8.10 (s, 1H), 9.89 (br, 1H), 10.20 (s, 1H); ^{13}C-NMR (DMSO-d_6, δ in ppm): 115.86, 118.97, 119.98, 127.13, 129.89, 138.97, 155.93, 156.50.

[Hsal-tch] (**II**) was prepared by adopting the method used to synthesize [Hsal-sch] (**I**).

Data for [Hsal-tch] (**II**): yield: 67.91% (1.32 g); anal. calcd for $C_8H_9N_3OS$ (MW 195.24); C, 49.21%; H, 4.65%; N, 21.52%. Found: C, 49.10%; H, 4.71%; N, 21.45%. FT-IR (ATR, cm^{-1}): 3430($\nu_{O\text{-}H}$), 3283($\nu_{N\text{-}H}$), 1604($\nu_{C=N}$), 1037($\nu_{C=S}$); UV–Vis [λ_{max} (nm), ε ($lmol^{-1}$ cm^{-1})]: 230 (1.13×10^3), 294 (sh), 304 (1.88×10^3), 331 (2.35×10^3). ^{1}H-NMR (DMSO-d_6, δ in ppm): 6.76–6.80 (t, 1H), 6.83–6.85 (d, 1H), 7.15–7.19 (t, 1H), 7.84 (s, 2H), 8.07 (s, 1H), 8.37 (s, 1H), 9.79 (s, 1H), 11.37 (s, 1H); ^{13}C-NMR (DMSO-d_6, δ in ppm): 115.91, 120.08, 126.55, 130.22, 132.35, 137.97, 154.08, 156.55.

2.5 | Synthesis of [H_2bissal-sch] (III) and [H_2bissal-tch] (IV)

A hot methanolic solution (25 ml) of 5,5′-methylenebis (2-hydroxybenzaldehyde) (H_2bissal) (2.5625 g, 10 mmol) was reacted with the methanolic solution (25 ml) of semicarbazide hydrochloride or thiosemicarbazide (20 mmol), and this reaction mixture was refluxed for 1 hr (Scheme 1). During refluxing, the white colored solid

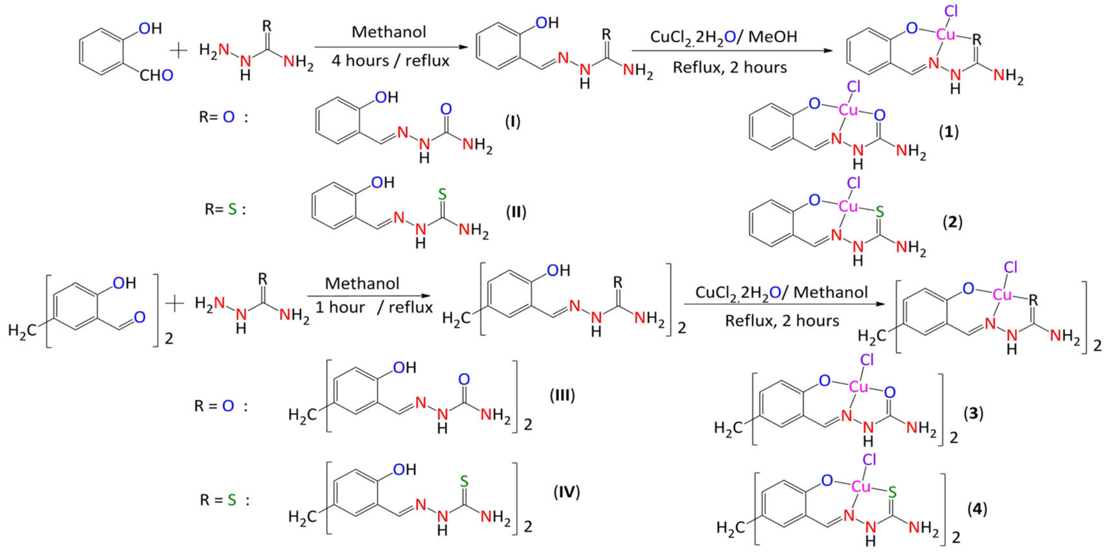

SCHEME 1 Proposed synthetic scheme for the preparation of ligands and their corresponding copper (II) complexes reported in this paper

product precipitated out, which was filtered, washed with ether, and dried in vacuum over silica gel.

Data for [H_2bissal-sch] (**III**): yield: 65.21% (1.82 g); anal. calcd for $C_{17}H_{18}N_6O_4$ (MW 370.36); C, 55.13%; H, 4.90%; N, 22.69%. Found: C, 55.08%; H, 5.01%; N, 22.55%. FT-IR (ATR, cm^{-1}): 3482($\nu_{O\text{-}H}$), 3273($\nu_{N\text{-}H}$), 1690($\nu_{C=O}$), 1583($\nu_{C=N}$); UV–Vis [λ_{max} (nm), ε ($lmol^{-1}$ cm^{-1})]: 221 (2.65×10^3), 281 (3.26×10^3), 289 (sh), 325 (1.63×10^3); ^{1}H-NMR (DMSO-d_6, δ in ppm): 3.72 (s, 2H), 6.27 (br, 4H), 6.71–6.73 (d, 2H), 6.93–6.96 (d, 2H), 7.50 (s, 2H), 8.06 (s, 2H), 9.67 (br, 2H), 10.12 (s, 2H); ^{13}C-NMR (DMSO-d_6, δ in ppm): 37.05, 116.04, 119.20, 120.06, 127.02, 130.94, 140.49, 156.42, 177.62.

Data for [H_2bissal-tch] (**IV**): yield; 81.25% (2.53 g); anal. calcd for $C_{17}H_{18}N_6O_2S_2$ (MW 402.49); C, 50.73%; H, 4.51%; N, 20.88%. Found: C, 50.69%; H, 4.71%; N, 20.75%. FT-IR (ATR, cm^{-1}): 3437($\nu_{O\text{-}H}$), 3278($\nu_{N\text{-}H}$), 1608($\nu_{C=N}$), 1039($\nu_{C=S}$); UV–Vis [λ_{max} (nm), ε ($lmol^{-1}$ cm^{-1})]: 235 (4.57×10^3), 298 (sh), 309 (6.20×10^3), 339 (6.44×10^3). ^{1}H-NMR (DMSO-d_6, δ in ppm): 3.69 (s, 2H), 6.70–6.73 (d, 2H), 7.00–7.03 (d, 2H), 7.92 (s, 4H), 8.04 (s, 2H), 8.30 (s, 2H), 9.53 (s, 2H), 11.33 (s, 2H). ^{13}C-NMR (DMSO-d_6, δ in ppm): 37.10, 116.10, 120.44, 126.42, 130.52, 132.71, 137.51, 154.15, 156.86.

2.6 | Synthesis of [Cu (sal-sch)Cl] (1), [Cu (sal-tch)Cl] (2), [CH_2{Cu (sal-sch)Cl}$_2$] (3) and [CH_2{Cu (sal-tch)Cl}$_2$] (4)

Complexes **1–4** were prepared by following a common synthetic route. [Cu (sal-sch)Cl] (**1**) and [Cu (sal-tch)Cl] (**2**) were prepared by reacting the methanolic solution of $CuCl_2 \cdot 2H_2O$ with [Hsal-sch] (**I**) and [Hsal-tch] (**II**) in 1:1 ratio, respectively. Likewise, [CH_2{Cu (sal-sch)Cl}$_2$] (**3**) and [CH_2{Cu (sal-tch)Cl}$_2$] (**4**) were isolated by reacting [H_2bissal-sch] (**III**) and [H_2bissal-tch] (**IV**) with $CuCl_2 \cdot 2H_2O$ in 1:2 ratio, respectively. During the synthesis of **1–4**, all the complexes separated out from the refluxing reaction mixture, which were filtered, washed with methanol (3 × 10 ml) and dried in vacuum over silica gel (Scheme 1).

2.6.1 | Data for [Cu (sal-sch)Cl] (1)

Yield: 78.34% (2.17 g); anal. calcd for $C_8H_8ClCuN_3O_2$ (MW 277.17): C, 34.67%; H, 2.91%; N, 15.16%. Found: C, 34.56%; H, 3.05%; N, 15.01%. FT-IR (ATR, cm^{-1}): 3344($\nu_{O\text{-}H}$), 3155($\nu_{N\text{-}H}$), 1648($\nu_{C=O}$), 1536($\nu_{C=N}$). UV–Vis [λ_{max} (nm), ε ($lmol^{-1}$ cm^{-1})]: 227 (4.32×10^3), 252 (3.43×10^3), 270 (2.94×10^3), 295 (2.49×10^3), 309 (1.76×10^3), 367 (2.19×10^3), 724 (91). ESI$^+$-MS: *m*/*z* 243.04 ([[Cu (sal-Hsch)] + H]$^+$).

2.6.2 | Data for [Cu (sal-tch)Cl] (2)

Yield: 82.04% (2.40 g); anal. calcd for $C_8H_8ClCuN_3OS$ (MW 293.23): C, 32.77%; H, 2.75%; N, 14.33%. Found: C, 32.66%; H, 2.91%; N, 14.17%. FT-IR (ATR, cm^{-1}): 3378($\nu_{O\text{-}H}$), 3250($\nu_{N\text{-}H}$), 1586($\nu_{C=N}$), 1026($\nu_{C=S}$). UV–Vis [λ_{max} (nm), ε ($lmol^{-1}$ cm^{-1})]: 207 (3.33×10^3), 230 (2.76×10^3), 270 (4.02×10^3), 321 (2.79×10^3), 353 (1.71×10^3), 385 (1.78×10^3), 641 (113). ESI$^+$-MS: *m*/*z* 258.98 ([Cu (sal-Htch)]$^+$).

2.6.3 | Data for [CH_2{Cu (sal-sch)Cl}$_2$] (3)

Yield: 61.32% (2.92 g); anal. calcd for $C_{17}H_{16}Cl_2Cu_2N_6O_4$ (MW 566.34); C, 36.05%; H, 2.85%; N, 14.84%. Found: C, 35.96%; H, 3.05%; N, 14.67%. FT-IR (ATR, cm^{-1}): 3401($\nu_{O\text{-}H}$), 3240($\nu_{N\text{-}H}$), 1654($\nu_{C=O}$), 1543($\nu_{C=N}$); UV–Vis [λ_{max} (nm), ε ($lmol^{-1}$ cm^{-1})]: 225 (4.76×10^3), 258 (3.83×10^3), 296 (sh), 313 (sh), 373 (1.45×10^3), 608 (398), 738(167); ESI^+-MS: *m*/*z* 566.11 ([CH_2{Cu (sal-sch) Cl}$_2$]$^+$), *m*/*z* 568.12 ([CH_2{Cu (sal-Hsch)Cl}$_2$]$^+$).

2.6.4 | Data for [CH_2{Cu (sal-tch)Cl}$_2$] (4)

Yield: 59.74% (3.03 g); anal. calcd for $C_{17}H_{16}Cl_2Cu_2N_6O_2S_2$ (MW 598.48); C, 34.12%; H, 2.69%; N, 14.04%. Found: C, 34.06%; H, 2.75%; N, 14.07%. FT-IR (ATR, cm^{-1}): 3374($\nu_{O\text{-}H}$), 3240($\nu_{N\text{-}H}$), 1588($\nu_{C=N}$), 1017($\nu_{C=S}$); UV–Vis [λ_{max} (nm), ε ($lmol^{-1}$ cm^{-1})]: 219 (1.72×10^3), 255 (1.62×10^3), 298 (1.61×10^3), 311 (sh), 328 (sh), 401 (5.90×10^2), 645 (337). ESI^+-MS: *m*/*z* 598.07 ([CH_2{Cu (sal-tch)Cl}$_2$]$^+$), *m*/*z* 600.07 ([CH_2{Cu (sal-Htch)Cl}$_2$]$^+$).

2.7 | General route for the preparation of PS-[Cu (sal-sch)Cl] (5), PS-[Cu (sal-tch)Cl] (6), PS-[CH_2{Cu (sal-sch)Cl}$_2$] (7) and PS-[CH_2{Cu (sal-tch)Cl}$_2$] (8)

Chloromethylated polystyrene-anchored metal complexes **5–8** were prepared by following a slightly modified method[15] from the literature, which is as follows.

In a 250-ml RB, chloromethylated polystyrene (1.0 g, 3.5–4.5 mmol/g Cl^-, 1% crosslinked with divinyl benzene) was allowed to swell in 10 ml DMF for 24 hr. DMF solution of KI (1.66 g, 10 mmol) was added to the above suspension followed by the addition of 20 ml DMF solution of complexes **1–4** (15 mmol), and the resultant mixture was heated at 150°C in an oil bath fitted with a water condenser and stirred for 48 hr. After cooling to room temperature, the dark colored polymer beads were filtered, washed with hot DMF solution, followed by water, methanol and dried in an air oven at 120°C for 24 hr (Scheme 2).

2.7.1 | Data for PS-[Cu (sal-sch)Cl] (5)

Recovery yield 98.76% (0.9876 g). FT-IR (ATR, cm^{-1}): 3787(trapped MeOH), 3346($\nu_{O\text{-}H}$), 3157($\nu_{N\text{-}H}$), 1644($\nu_{C=O}$), 1532($\nu_{C=N}$); UV–Vis (Nujol, nm): 203, 224, 302, 370.

2.7.2 | Data for PS-[Cu (sal-tch)Cl] (6)

Recovery yield 99.06% (0.9906 g). FT-IR (ATR, cm^{-1}): 3721(trapped MeOH), 3347($\nu_{O\text{-}H}$), 3256($\nu_{N\text{-}H}$), 1590($\nu_{C=N}$), 1015($\nu_{C=S}$); UV–Vis (Nujol, nm): 205, 221, 275, 486.

2.7.3 | Data for PS-[CH_2{Cu (sal-sch)Cl}$_2$] (7)

Recovery yield 97.86% (0.9786 g). FT-IR (ATR, cm^{-1}): 3736(trapped MeOH), 3415($\nu_{O\text{-}H}$), 3228($\nu_{N\text{-}H}$), 1671 ($\nu_{C=O}$), 1546($\nu_{C=N}$); UV–Vis (Nujol, nm): 201, 227, 319, 386.

2.7.4 | Data for PS-[CH_2{Cu (sal-tch)Cl}$_2$] (8)

Recovery yield 98.45% (0.9845 g). FT-IR (ATR, cm^{-1}): 3771(trapped MeOH), 3366($\nu_{O\text{-}H}$), 3237($\nu_{N\text{-}H}$), 1580 ($\nu_{C=N}$), 1010($\nu_{C=S}$). UV–Vis (Nujol, nm): 203, 226, 268, 404.

2.8 | Catalytic activity

The catalytic activities of **5–8** were tested against the oxidation of various aromatic and aliphatic alkenes – cyclohexene, *cis*-cyclooctene, styrene, 1-methylcyclohexene and 1-hexene. In a typical reaction, 10 ml methanolic

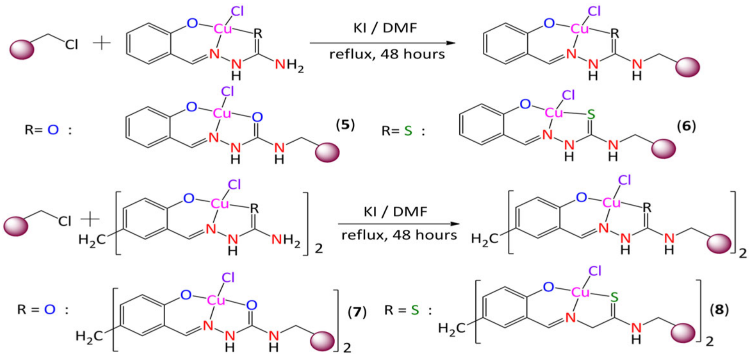

SCHEME 2 Proposed synthetic route for the preparation of polymer-grafted copper (II) complexes

solution of cyclohexene (0.415 g, 5 mmol) was reacted with a dilute aqueous solution of 30% H_2O_2 (2.28 g, 20 mmol) in the presence of pre-swelled catalyst **5–8** (40 mg) at 70°C for 6 hr. All the catalysts were swelled in methanol for 12 hr before being used. Small aliquots of the reaction mixture were withdrawn periodically and quantitatively measured by a GC. To optimize the catalytic reaction for obtaining maximum % conversion, the impacts of various parameters such as catalyst amount, oxidant amount, solvent amount and nature of solvent were checked. Under the optimized reaction conditions, catalytic oxidation of other substrates was also examined and analyzed through GC periodically. The products were identified by GC–MS fitted with a TG-5MS capillary column. The % conversion of the substrates and % selectivity of the products were calculated by using equations (1) and (2).

$$\%\text{Conversion of substrate} = 100 - \frac{Area\ of\ substrate}{Total\ area\ of\ substrate + Area\ of\ products} \times 100 \quad (1)$$

$$\text{Similarly, } \%\text{Selectivity} = 100 - \frac{Area\ of\ product}{Total\ area\ of\ products} \times 100 \quad (2)$$

3 | RESULTS AND DISCUSSION

3.1 | Infrared spectroscopy

Infrared spectroscopy was used to analyze all the ligands [Hsal-sch] (**I**), [Hsal-tch] (**II**), [H_2bissal-sch] (**III**) and [H_2bissal-tch] (**IV**), along with their corresponding copper complexes [Cu (sal-sch)Cl] (**1**), [Cu (sal-tch)Cl] (**2**), [CH_2{Cu (sal-sch)Cl}$_2$] (**3**) and [CH_2{Cu (sal-tch)Cl}$_2$] (**4**). FT-IR spectra of ligands **I–IV** are presented in Figure S1, whereas Figure S2 displays the FT-IR spectra of complexes **1–4.** Selected FT-IR data of ligands **I–IV** and complexes **1–4** are shown in Table 1. Despite the presence of secondary amine (-NH), primary amine (-NH_2) and aromatic hydroxyl (-OH) groups in the ligands **I–IV**, only two prominent bands appear in the range of 3273 cm^{-1} to 3482 cm^{-1}. Relatively sharp bands arising in the range of 3273 cm^{-1} to 3283 cm^{-1} are assigned to $\nu_{(N\text{-}H)}$.[16] The $\nu_{(O\text{-}H)}$ stretch is designated to the bands occurring in the range 3430 cm^{-1} to 3482 cm^{-1}.[17,18]

Upon complexation, the $\nu_{(N\text{-}H)}$ stretching frequency shifted to a lower wavenumber. The shift in $\nu_{(N\text{-}H)}$ ($\Delta\nu_{(N\text{-}H)}$) is 33 cm^{-1} in (**2**), 33 cm^{-1} in (**3**) and 38 cm^{-1} in (**4**), and indicates bonding between metal and ligands, while exceptional large shifting ($\Delta\nu_{(N\text{-}H)} = 119$ cm^{-1}) of $\nu_{(N\text{-}H)}$ in (**1**) is attributed to the strong H-bonding interaction between -NH of ligand and water of crystallization along with the bonding interaction with the metal. The absence of phenolic -OH group in complexes **1–4** discloses the -NH_2 band at 3344 cm^{-1} (**1**), 3378 cm^{-1} (**2**), 3401 cm^{-1} (**3**) and 3374 cm^{-1} (**4**). In the polymer-supported metal complexes **5–8**, the $\nu_{(N\text{-}H)}$ stretch appears in the range of 3157–3256 cm^{-1}, while the -NH_2 stretching band appears at 3346 cm^{-1} (**5**), 3347 cm^{-1} (**6**), 3415 cm^{-1} (**7**) and 3366 cm^{-1} (**8**). Apart from these bands, all the polymer-anchored metal complexes, as well as recycled complexes, exhibit one band in the range of 3709 to 3787 cm^{-1} due to the presence of trapped methanolic -OH group (Figure S3). The ligands show a sharp band at 1581 cm^{-1} (**I**), 1604 cm^{-1}(**II**), 1583 cm^{-1} (**III**) and 1608 cm^{-1} (**IV**), which is attributed to $\nu_{(C=N)}$. These bands switched to the lower wavelength in complexes **1–4**, implies coordination of azomethine nitrogen to the copper center. The

TABLE 1 Selected FT-IR data of the ligands **I–IV**, copper (II) complexes **1–4** and polymer-anchored copper (II) complexes **5–8** in cm^{-1}

S.N.	Compounds	$\nu_{C=N}$	$\nu_{C=O}$	$\nu_{C=S}$	$\nu_{N\text{-}H}$	$\nu_{O\text{-}H}$	ν_{NH2}	ν_{CH3OH}
1.	[Hsal-sch] (**I**)	1581	1684	–	3274	3479	–	–
2.	[Hsal-tch] (**II**)	1604	–	1037	3283	3430	–	–
3.	[H_2bissal-sch] (**III**)	1583	1690	–	3273	3482	–	–
4.	[H_2bissal-tch] (**IV**)	1608	–	1039	3278	3437	–	–
5.	[Cu (sal-sch)Cl] (**1**)	1536	1648	–	3155	–	3344	–
6.	[Cu (sal-tch)Cl] (**2**)	1586	–	1026	3250	–	3378	–
7.	[CH_2{Cu (sal-sch)Cl}$_2$] (**3**)	1543	1654	–	3240	–	3401	–
8.	[CH_2{Cu (sal-tch)Cl}$_2$] (**4**)	1588	–	1017	3240	–	3374	–
9.	PS-[Cu (sal-sch)Cl] (**5**)	1532	1644	–	3157	–	3346	3787
10.	PS-[Cu (sal-tch)Cl] (**6**)	1590	–	1015	3256	–	3347	3721
11.	PS-[CH_2{Cu (sal-sch)Cl}$_2$] (**7**)	1546	1671	–	3228	–	3415	3736
12.	PS-[CH_2{Cu (sal-tch)Cl}$_2$] (**8**)	1580	–	1010	3237	–	3366	3771

$\nu_{(C=O)}$ bands of the ligands become visible at 1684 cm^{-1}(**I**) and 1690 cm^{-1} (**III**). The presence of $\nu_{(C=O)}$ bands in the ligands (**I**) and (**III**) indicates their existence in keto form over the enol form in the solid state. In the ligands, bands appearing at 1037 cm^{-1}(**II**) and 1039 cm^{-1} (**IV**) are due to $\nu_{(C=S)}$.[19] In complexes (**1**) and (**3**), keto >C=O band appears at 1648 and 1654 cm^{-1}, respectively, while the >C=S band is present at 1026 and 1017 cm^{-1} in complexes (**2**) and (**4**), respectively, indicating coordination of the oxygen of >C=O group and the sulfur of >C=S group to the copper center. All of these characteristic bands are clearly visible in the polymer-anchored complexes (shown in Figure S4) with slight shifting from their original position, which symbolizes successful covalent attachment of the metal complexes in the polymeric chain.

3.2 | UV–Vis spectral analysis

Electronic absorption spectra of the ligands (**I**)–(**IV**) and copper complexes (**1**)–(**4**) were analyzed by employing a UV–Vis spectrophotometer using MeOH/DMF as solvent at room temperature, and are shown in Figure S5. Electronic spectra of polymer-anchored copper complexes **5–8** along with the recycled complexes **5′–8′** were recorded in Nujol and are shown in Figure S6. All the λ_{max} values along with the molar extinction coefficients (ε) are shown in Table 2. The electronic spectral pattern of ligand [Hsal-sch] (**I**) appears to be similar to that of ligand [H$_2$bissal-sch] (**III**), and the electronic spectral pattern of ligand [Hsal-tch] (**II**) shows a close resemblance with ligand [H$_2$bissal-tch] (**IV**), which indicates their close structural similarities as evident from their molecular structures.

Ligand (**I**) shows three spectral bands at 216 nm, 277 nm and 317 nm along with two shoulder bands, one at 224 nm and another at 286 nm, whereas ligand (**III**) displays these bands at 221 nm, 281 nm and 325 nm in association with only one shoulder band at 289 nm. The most feasible assignment for these bands is σ-σ^*, π_1-π_1^*, π_2-π_2^* and n-π^* transitions, respectively. On the other hand, ligand (**II**) exhibits 230 nm, 304 nm and 331 nm bands accompanied with one shoulder band at 294 nm in its electronic spectrum, while ligand (**IV**) shows these bands at 235 nm, 309 nm and 339 nm coupled with one shoulder band at 298 nm. The most possible designation of these bands is σ-σ^*, π_1-π_1^*, π_2-π_2^* and π_3-π_3^*, respectively. Metal complexes (**1**)–(**4**) carry all the signature bands of corresponding ligands slightly shifted from their original positions. The complexes display a medium to intense band at 367 nm (**1**), 385 nm (**2**), 373 nm (**3**) and 401 nm (**4**) due to the ligand to metal charge transfer transition from phenolate oxygen to *d*-orbitals of copper (II) along with a partial contribution from n-π^* transition.[20] The copper (II) complexes exhibit a medium intensity band

TABLE 2 Electronic spectral data (recorded in MeOH/DMF/Nujol) of the ligands (**I–IV**), copper (II) complexes (**1–4)** and polymer-anchored copper (II) complexes (**5–8**), along with λ_{max} and molar extinction coefficient

S.N.	**Compounds**	**Solvent**	λ_{max} **(nm),** ε **(lmol^{-1} cm^{-1})**
1.	[Hsal-sch] (**I**)	MeOH	216 (2.07 × 10^3), 224[a], 277 (2.41 × 10^3), 286[a], 317 (1.48 × 10^3)
2.	[Hsal-tch] (**II**)	MeOH	230 (1.13 × 10^3), 294[a], 304 (1.88 × 10^3), 331 (2.35 × 10^3)
3.	[H$_2$bissal-sch] (**III**)	MeOH	221 (2.65 × 10^3), 281 (3.26 × 10^3), 289[a], 325 (1.63 × 10^3)
4.	[H$_2$bissal-tch] (**IV**)	MeOH	235 (4.57 × 10^3), 298[a], 309 (6.20 × 10^3), 339 (6.44 × 10^3)
5.	[Cu (sal-sch)Cl] (**1**)	MeOH	227 (4.32 × 10^3), 252 (3.43 × 10^3), 270 (2.94 × 10^3), 295 (2.49 × 10^3), 309 (1.76 × 10^3), 367 (2.19 × 10^3), 724* (91)
6.	[Cu (sal-tch)Cl] (**2**)	MeOH	207 (3.33 × 10^3), 230 (2.76 × 10^3), 270 (4.02 × 10^3), 321 (2.79 × 10^3), 355 (1.71 × 10^3), 385 (1.78 × 10^3), 641* (113)
7.	[CH$_2${Cu (sal-sch)Cl}$_2$] (**3**)	MeOH	225 (4.76 × 10^3), 258 (3.83 × 10^3), 296[a], 313[a], 373 (1.45 × 10^3), 608* (398), 738* (167)
8.	[CH$_2${Cu (sal-tch)Cl}$_2$] (**4**)	MeOH	219 (1.72 × 10^3), 255 (1.62 × 10^3), 298 (1.61 × 10^3), 311[a], 328[a], 401 (5.90 × 10^2), 645* (337)
9.	PS-[Cu (sal-sch)Cl] (**5**)	Nujol	203, 224, 302, 370
10.	PS-[Cu (sal-tch)Cl] (**6**)	Nujol	205, 221, 275, 486
11.	PS-[CH$_2${Cu (sal-sch)Cl}$_2$] (**7**)	Nujol	201, 227, 319, 386
12.	PS-[CH$_2${Cu (sal-tch)Cl}$_2$] (**8**)	Nujol	203, 226, 268, 404

**d-d* transition (recorded in DMF).

[a] shoulder band.

in the range of 608–738 nm attributed to *d-d* transitions (shown in Figure S7). The electronic spectra of polymer-anchored metal complexes (**5**)–(**8**) show quite low intense absorbance bands (shown in Figure S6) because of poor metal loading into the polymeric chain. Although it is very hard to assign the true nature of the electronic transitions visible in polymer-anchored metal complexes, the presence of these transitions definitely indicates the presence of copper complexes in the polymeric matrix.

3.3 | Nuclear magnetic resonance study

To establish the molecular structure of ligands (**I**)–(**IV**) in solution, ^{1}H-NMR analysis was performed and their spectra are presented in Figure 1. Ligand (**I**) produces almost identical ^{1}H-NMR spectrum to that of (**III**), and ligand (**II**) also demonstrates the similar spectral pattern with (**IV**) due to their close similarity in molecular structures. Moreover, proton signals displayed by (**III**) and (**IV**) are equivalent to that of the signals observed in ligands (**I**) and (**II**), except for the signal of >CH_2 (methylene) protons. The chemical shift of all the protons of ligands (**I**)–(**IV**) are summarized in Table S1, which supports the FT-IR data acquired in the solid state of the ligands. A singlet signal emerges at 10.20 ppm (**I**), 11.37 ppm (**II**), 10.12 ppm (**III**) and 11.33 ppm (**IV**) due to the phenolic -OH proton. The proton signal of -NH group of ligands (**I**)–(**IV**) appears at 9.89 ppm, 9.79 ppm, 9.67 ppm and 9.53 ppm, respectively.

Ligands (**I**) and (**III**) display the -NH_2 protons signal in the range of 6.24–6.27 ppm, whereas ligands (**II**) and (**IV**) show the same proton resonance in the range of 7.84–7.92 ppm. One sharp singlet signal characteristic of azomethine (–CH=N–) proton appears in the range of 8.10–8.06 ppm in (**I**) and (**III**), while the same signal was produced by (**II**) and (**IV**) in the range of 8.37–8.30 ppm.[20,21] In the ligands (**I**)–(**IV**) aromatic protons appear in the expected range. Besides this, (**III**) and (**IV**) exhibit one additional proton signal due to the >CH_2 (methylene) protons at 3.72 ppm and 3.69 ppm, respectively.[19]

^{13}C-NMR spectroscopy was used to confirm the molecular frame of (**I**)–(**IV**). ^{13}C-NMR spectra of (**I**)–(**III**) were recorded in a mixture of $CDCl_3$/DMSO-d_6, while ligand (**IV**) was analyzed in DMSO-d_6 only (shown in Figure 2). As expected, (**I**) and (**II**) show eight (08) distinctive signals in their ^{13}C-NMR spectra, whereas nine (09) signals are observed for (**III**) and (**IV**). The observed signals and their assignments are shown in Table S2, which are in good agreement with the molecular structure proposed by FT-IR and ^{1}H-NMR analyses. Ligands (**I**) and (**III**) show ^{13}C signal of >C=O (C8) group at 156.50 ppm and 177.62 ppm, while (**II**) and (**IV**) exhibit the ^{13}C signal of the same carbon atom of the >C=S group at 156.55 ppm and 156.86 ppm, respectively.

The ligands (**I**)–(**IV**) produce a ^{13}C signal of phenolic OH group (C1) at 155.93 (**I**), 154.08 (**II**), 156.42 (**III**) and 154.15 ppm (**IV**), whereas azomethine (>C=N) signal appears at 138.97, 137.97, 140.49 and 137.51 ppm, respectively. The signals due to the aromatic carbons appear in the expected region in the ligands (**I**)–(**IV**). One aliphatic ^{13}C signal is shown by (**III**) and (**IV**) at 37.05 ppm and 37.10 ppm, respectively, because of the methylene group (>CH_2).[19–21]

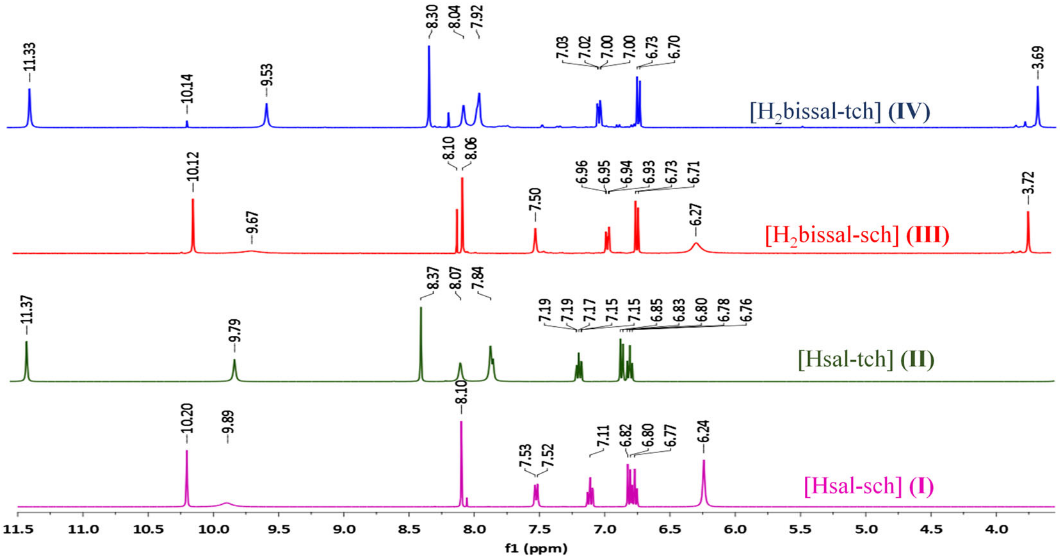

FIGURE 1 ^{1}H-NMR spectra of [Hsal-sch] (**I**), [Hsal-tch] (**II**), [H_2bissal-sch] (**III**) and [H_2bissal-tch] (**IV**) recorded in DMSO-d_6

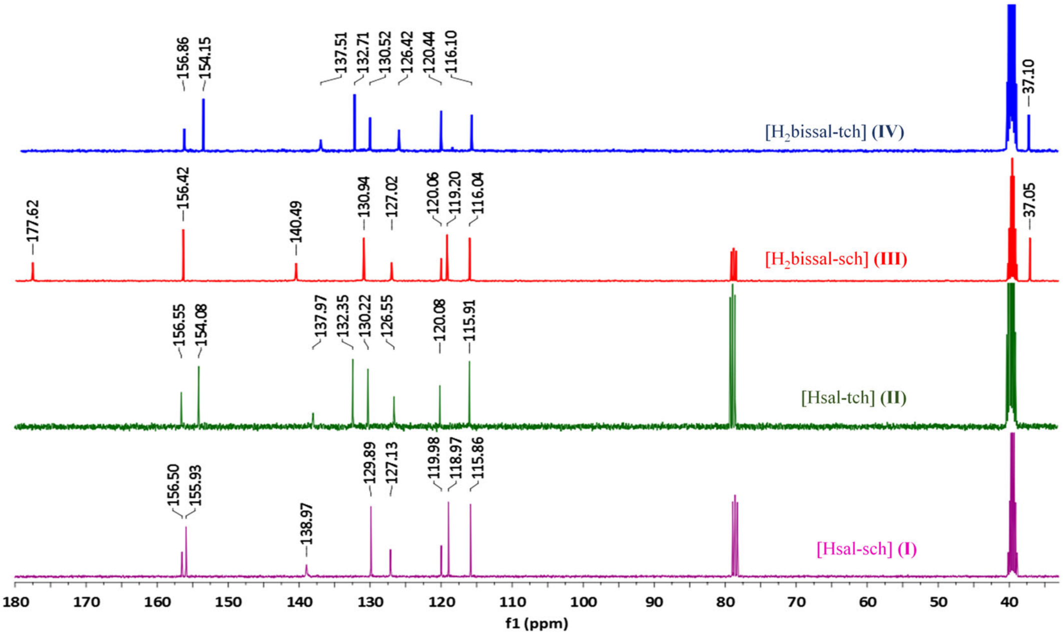

FIGURE 2 ^{13}C-NMR spectra of [Hsal-sch] (**I**), [Hsal-tch] (**II**), [H$_2$bissal-sch] (**III**) and [H$_2$bissal-tch] (**IV**) recorded in DMSO-d_6

3.4 | EPR analysis

The X-band EPR spectra of Cu^{II} complexes **1–4** were recorded in DMSO at room temperature and presented in Figure 3(a), whereas room temperature EPR spectra of polymer-anchored Cu^{II} complexes **5–8** are shown in Figure 3(b). All the complexes show typical axial spectra with $g\parallel_{g(z)>}g\perp_{g(x)\,\approx\,g(y)} > g_e$, which is characteristic of a distorted square planar or square pyramidal Cu^{II} center with the $d_{x^2-y^2}$ ground state.[22–25] Computer-simulated spectra [shown by colored lines in Figure 3(a) and (b)] and Hamiltonian parameters are listed in Table S3.

In strong coordinating solvents, like DMSO, neat complexes adopt square pyramidal geometry, whereas in

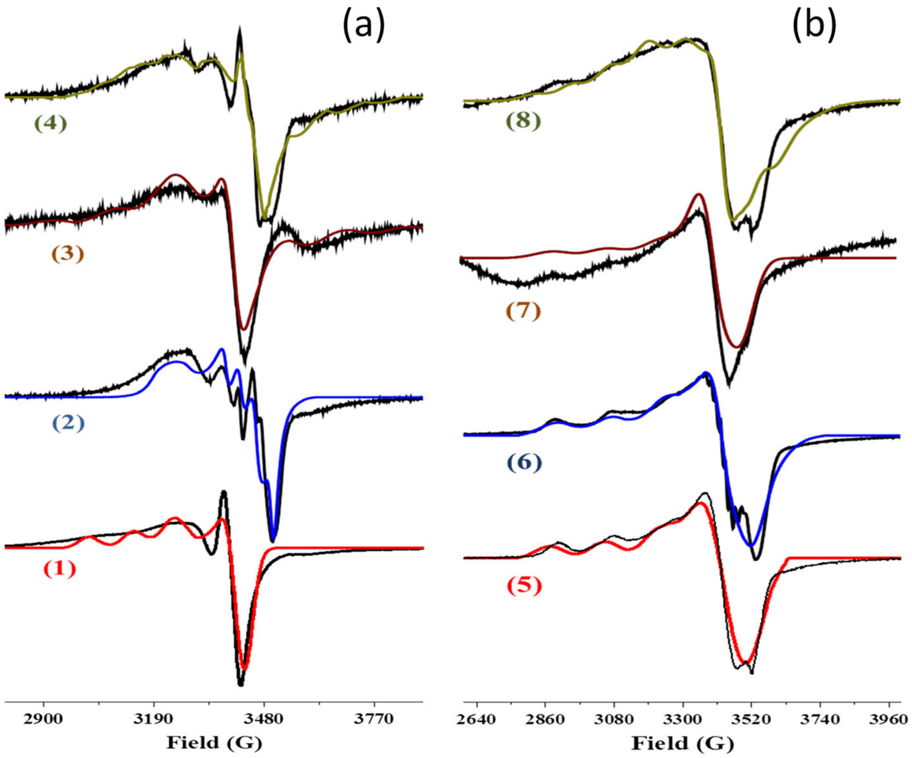

FIGURE 3 X-band electron paramagnetic resonance (EPR) spectra of (a) neat Cu^{II} complexes **1–4** in DMSO solution and (b) polymer-anchored Cu^{II} complexes **5–8** in solid state at room temperature

polymer matrix copper (II) complexes exist in square planar geometry. This structural difference is evident in EPR spectral patterns and *g*-values. Hyperfine splitting in the neat complexes **1–4** in DMSO solution could not be resolved at room temperature due to the rapid intermolecular copper–copper interaction in solution.[22,26] The absence of half field transition (~16 000 *G*) signifies the presence of a monomeric form of neat complexes in solution.

However, polymer-anchored Cu^{II} complexes produce clearly resolved hyperfine splitting in parallel region. In the complexes, these hyperfine lines split g‖ signals with an average spacing of 170 *G*. A well-resolved hyperfine spectrum indicates that the Cu^{II} complexes are excellently distributed into the polymer matrix without significant copper–copper magnetic interaction. On the other hand, the perpendicular region of the spectra is not well resolved, although they exhibit poorly resolved superhyperfine splitting due to the presence of coordinating nitrogen of the ligand.

3.5 | Computational analysis

3.5.1 | Optimization

To visualize solid state molecular structure as well as to recognize the chemical properties of a molecule, the theoretical calculation is an influential leading technique. Among complexes **1–4**, only complex **1** is isolated as a single crystal.[14] Due to the lack of single crystal XRD data for complexes **2**, **3** and **4**, the ground state molecular structure of these complexes was derived from geometry optimization by using mixed basis set DFT/B3LYP/LANL2DZ∪ 6–311 + G(d, p) (shown in Figure S8). Experimental values along with the optimized theoretical values of selected bond angles and bond lengths are listed in Table S4.

Among important bond distances, the maximum deflection of 0.153 Å is observed in Cu1-O1, whereas among calculated bond angles, the maximum difference of 6.72° is observed in O1-Cu1-O2 angle from the experimental value. Besides these differences, as stated in Table S4, theoretically calculated parameters of complex **1** are in close agreement to those acquired from X-ray crystallographic analysis. Hence, theoretically calculated structural parameters and geometry of the complexes **2–4** truly represent their solid state form like complex **1**. However, a little fluctuation between DFT calculated and experimental data can be addressed by the fact that experimental parameters were obtained in solid states while DFT calculated data are obtained by using a single molecule in gaseous states in the absence of lattice interactions. Frontier molecular orbitals play a key role in predicting the optical and electrical properties of the molecules. According to Koopmans' theorem, IP $\approx -\epsilon_{HOMO}$ and EA $\approx -\epsilon_{LUMO}$, this works out reasonably well numerically for organic molecules. Hence, HOMO and LUMO can be used to predict Mulliken's electronegativity (χ), which is an average value of HOMO and LUMO energies. Moreover, the difference between HOMO and LUMO energies reflects the hardness (η) of a molecule. And to estimate the kinetic stability as well as chemical reactivity of the molecules, electronegativity (χ) and hardness (η) of the molecule are often used unanimously. But in DFT, simply considering HOMO/LUMO energy values as IP/EA does not work well numerically. Hence, by performing total energy calculation of ionic systems, we have calculated vertical ionization potential (IP_v) and vertical electron affinity (EA_v).[27] Based on directly calculated IP_v and EA_v, fundamental quantum chemical properties like χ (electronegativity), hardness (η), ξ (softness), ψ (electrophilicity index), etc. have been estimated and listed in Table 3.

3D plots of HOMO and LUMO for molecules **1–4** are displayed in Figures S9–S12. According to Figures S9 and S10, in complexes **1** and **2** α-HOMO surfaces are spread almost over the entire molecule, except for O1/S1 and metal (Cu1) atoms. Similarly, α-LUMO is also located over the entire molecule, although Cll atom does not have any orbital contribution and a small orbital contribution comes from the metal (Cu1) towards α-LUMO. Both complexes **1** and **2** show close similarities between α-HOMO and β-HOMO surface diagrams, but α-LUMOs of complexes **1** and **2** are distinctly different from their β-LUMO surface patterns (Figures S9 and S10). In HOMO and LUMO of complexes **3** and **4**, the atomic orbital contribution from coordinating heteroatoms is very little, except S1 (8.73% in HOMO and 9.43% in LUMO) in complex **4**. Hence, MO surfaces are distributed over metal and rest of the ligand in complexes **3** and **4**. Details of atomic orbital % in constructing the HOMO and LUMO in **1–4** are shown in Figures S13 and S14.

3.6 | TGA and atomic absorption spectroscopy analysis

Simultaneous DTA-TGA analysis plots of polymer-anchored Cu^{II} complexes **5–8** are presented in Figure S15. The DTA-TGA analysis was performed in the range 40–750°C under a nitrogen atmosphere using 20°C/min heating ramp.

Also, to monitor the impact of temperature on the polymer-anchored metal complexes, DTG plots of all the polymer-supported metal complexes are shown in Figure S16. All the supported complexes **5–8** undergo thermal decomposition via three major steps, which are a typical TGA pattern for polymer-supported metal

TABLE 3 Quantum chemical properties calculated by using DFT/B3LYP methods with mixed basis set LANL2DZ ∪ 6-311+G (d, p)

S. N.	Parameters	Complexes (1)	(2)	(3)	(4)
1	HOMO (eV)	-6.0192^{α} -5.9620^{β}	-5.9756^{α} -5.9266^{β}	−5.3117	−5.2083
2	LUMO (eV)	-2.3157^{α} -3.7171^{β}	-2.4708^{α} -3.5946^{β}	−4.8763	−4.8735
3	|E|(eV) (HOMO-LUMO energy gap)	3.7034^{α}	3.5048^{α}	0.4353	0.3347
4	IP (eV)	8.3474	7.9912	5.8855	5.7333
5	EA (eV)	−1.8064	−1.8704	−2.0836	−3.9555
6	χ (eV) (electronegativity)	3.2705	3.0604	1.9009	0.8889
7	η (eV) (chemical hardness)	5.0769	4.9308	3.9845	4.8444
8	ξ (eV) (softness)	0.0984	0.1014	0.1254	0.1032
9	ψ (eV) (electrophilicity index)	1.0534	0.9497	0.4534	0.0815

α = α-Molecular orbital; β = β-Molecular orbital

complexes, although these steps are overlapping in **5**. Complex **5** is thermally stable up to 300°C, whereas complexes **6–8** exhibit thermal stability up to 315°C, 300°C and 335°C, respectively. During this period, a small but progressive mass loss of 1.6%, 2.51%, 2.50% and 3.90% was recorded in the DTA plot by complexes **5–8**, respectively. This is because of the elimination of adsorbed gases and water molecules from the polymeric matrix.[16,22,28] In its second step, an exothermic thermal decomposition is observed in the range of 353–373°C by complexes **5–8** with an average mass loss of 27–47%, due to the melting of polymeric backbone along with the expulsion of Cl and a small fraction of ligand moiety. In its third and final step, a massive 49–53% of the mass elimination originated in the DTG plots of the supported complexes in the temperature range 505–527°C because of the complete decomposition of the ligand as well as the polymeric chain. However, in complex **5,** this mass change proceeds with two successive temperatures, one at 420°C and another at 587°C. Approximate metal content was also estimated and listed in Table 4.

The copper percentage in the metal complex grafted polymers was confirmed by atomic absorption spectroscopy (AAS) by decomposing the polymer-anchored metal complexes **5–8** with concentrated HNO_3 and subsequently diluting the filtrate with deionized water. The metal ion loading in the polymer was estimated by using equation (3).[29] PS-[Cu (sal-sch)Cl] (**5**), PS-[Cu (sal-tch)Cl] (**6**), PS-[CH_2{Cu (sal-sch)Cl}$_2$] (**7**) and PS-[CH_2{Cu (sal-tch)Cl}$_2$] (**8**) show copper loading of 0.11753 mmol/g, 0.07591 mmol/g, 0.25871 mmol/g and 0.16309 mmol/g, respectively (displayed in Table 4).[29]

$$\text{Metal ion loading} = \frac{\text{Observed metal}\% \times 10}{\text{Atomic weight of metal}} \qquad (3)$$

3.7 | SEM and EDX analysis

Surface morphology of the pure polymer, catalyst grafted polymers **5–8** and recycled ones were also examined by SEM and are shown in Figure 4. SEM image of pure chloromethylated polystyrene is reproduced from our previous work.[22] During the covalent anchoring of Cu^{II} complexes **1–4** into polymer matrix, morphological changes were monitored by scrutinizing the SEM image

TABLE 4 Metal ion loading in complexes **5–8**

S.N.	Catalysts	AAS Metal %	Metal loading (mmolg^{-1} of resin)	EDX	TGA
1	PS-[Cu (sal-sch)Cl] (**5**)	0.7469	0.11753	1.8742	–
2	PS-[Cu (sal-tch)Cl] (**6**)	0.4824	0.07591	2.3542	1.9830
3	PS-[CH_2{Cu (sal-sch)Cl}$_2$] (**7**)	1.6440	0.25871	2.9254	–
4	PS-[CH_2{Cu (sal-tch)Cl}$_2$] (**8**)	1.0364	0.16309	5.8996	0.2880

AAS, atomic absorption spectroscopy; EDX, energy-dispersive X-ray analysis; TGA, thermogravimetric analysis.

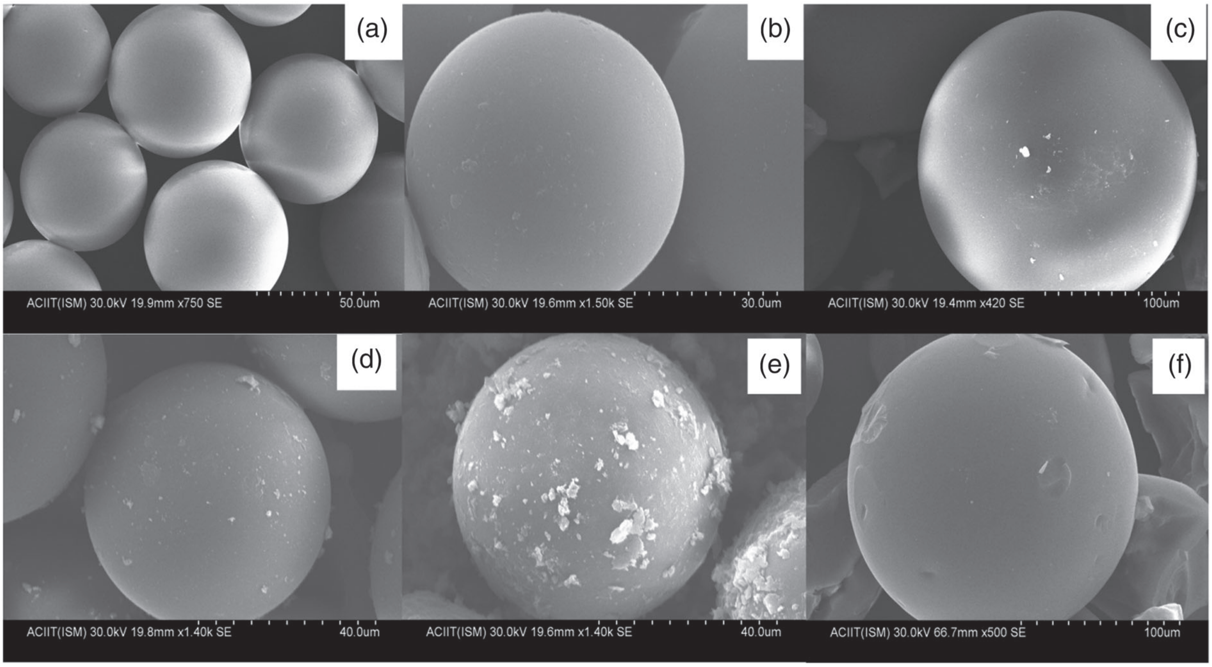

FIGURE 4 Scanning electron microscopy (SEM) images of: (a) pure chloromethylated polystyrene; (b) PS-[Cu (sal-sch)Cl] (**5**); (c) PS-[Cu (sal-tch)Cl] (**6**); (d) PS-[CH_2{Cu (sal-sch)Cl}$_2$] (**7**); (e) PS-[CH_2{Cu (sal-tch)Cl}$_2$] (**8**); and (f) recycled PS-[Cu (sal-tch)Cl] (**6**)

of a single bead of pure and metal complex grafted polymer. As predicted, the flat and glossy upper surface of pure polymer produces slight roughening in the metal complex grafted polymers **5–8** because of the covalent interaction of Cu^{II} complexes **1–4** with the polymer chain at various sites. This roughness is reduced in recycled metal complex anchored polymer beads (Figure 4f).

Additionally, to identify the elemental composition of the copper (II) complex-anchored polymers, EDX was performed and shown in Figure 5. Grafted polymers **5–8** contain a significant amount of copper along with C, O, and N (shown in Figure 5), indicating the existence of the metal complexes in the polymeric chain along with the ligand moiety. Complexes **6** and **8** show intense sulfur signals because of the presence of coordinating S atom in the ligand. A considerable amount of Cl signal (in the range of 0.17–3.7 weight %) was identified in the EDX plot of all the supported polymer beads, indicating the low concentration of Cu centers along with the different degree of copper loading into the polymer chain. EDX analysis estimated 1.8742, 2.3542, 2.9254 and 5.8996 mmol copper per gram of resin present in **5**, **6**, **7** and **8**, respectively (listed in Table 4).

3.8 | AFM analysis

Change in surface roughness was monitored by AFM during the course of heterogenization of the neat complexes **1–4** and displayed in Figure S17. Detailed surface roughness along with the mean height of all the complexes **5–8** are listed in Table S5.

The estimated average surface roughness and mean height of the pure chloromethylated polystyrene beads are 10.1 nm and 78.0 nm, respectively. While reacting with metal complexes **1–4**, the surface roughness, as well as mean height of pure PS-Cl, reduces. By reacting PS-Cl with **1–4**, surface roughness reduces to 5.94 nm, 6.80 nm, 3.86 nm and 4.04 nm, respectively. This is because of the fact that through covalent attachment of neat complexes into the polymer matrix, beads pores are occupied by complexes and hence reduces the porosity and consequently roughness is reduced.[30–33] The extent of roughness reduction can be correlated with the higher metal complex loading into the pore of the polymer beads. The observed roughness data as measured by AFM were in agreement with AAS analysis.

3.9 | Oxidation of alkenes

The parent catalysts PS-[Cu (sal-sch)Cl] (**5**), PS-[Cu (sal-tch)Cl] (**6**), PS-[CH_2{Cu (sal-sch)Cl}$_2$] (**7**) and PS-[CH_2{Cu (sal-tch)Cl}$_2$] (**8**) were used against the catalytic oxidation of a series of alkenes, namely cyclohexene, *cis*-cyclooctene, styrene, 1-methyl cyclohexene and 1-hexene in the presence of 30% hydrogen peroxide at 70°C temperature. All the alkenes produced the expected oxidation products along with a minor amount of unidentified products. Maximum oxidation of alkenes was obtained by optimizing

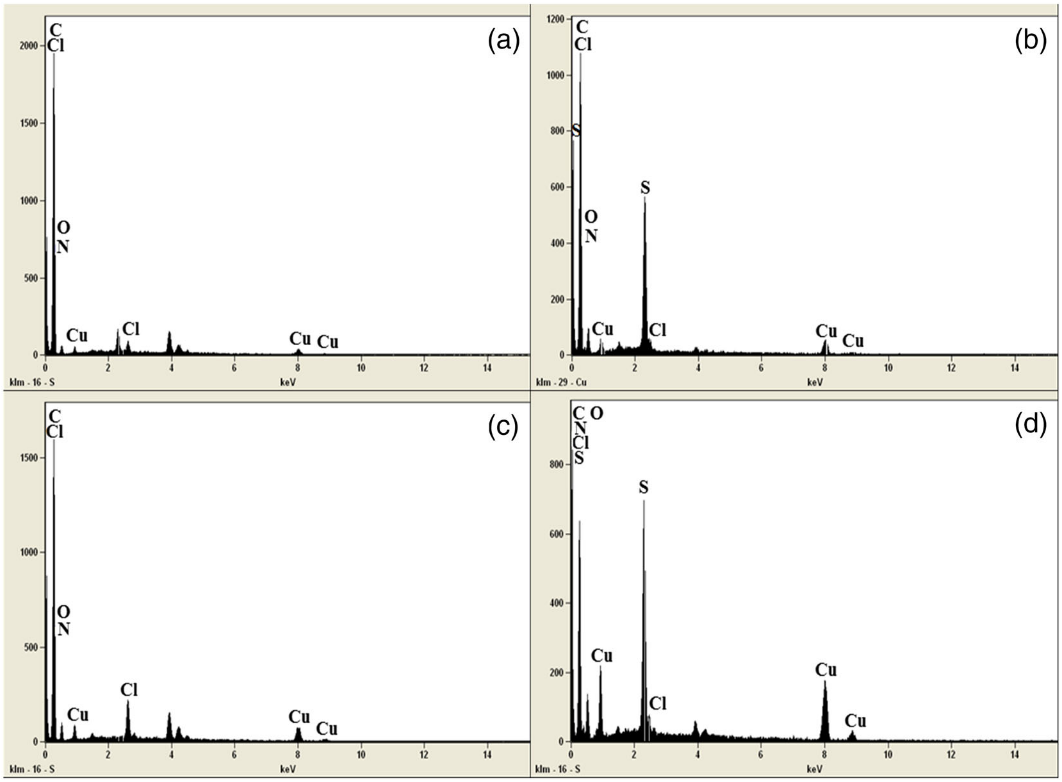

FIGURE 5 Energy-dispersive X-ray analysis (EDX) plots of: (a) PS-[Cu (sal-sch)Cl] (**5**); (b) PS-[Cu (sal-tch)Cl] (**6**); (c) PS-[CH_2{Cu (sal-sch) Cl}$_2$] (**7**); and (d) PS-[CH_2{Cu (sal-tch)Cl}$_2$] (**8**)

various reaction parameters, namely amount of parent catalyst, oxidant, solvent and nature of solvent by employing catalyst **6** and cyclohexene as a typical catalyst precursor and substrate, respectively. All the polymer grafted copper complexes were swelled in methanol for 12 hr before using them as a catalyst.

As reported in literature[34–39], oxidation of cyclohexene by H_2O_2 gave mainly cyclohexene oxide (Cyox), cyclohex-2-enol (2-cyclohexenol, Hexnol), cyclohexane-1,2-diol (Hexdiol), cyclohex-2-enone (Hexnon) and 2-hydroxycyclohexan-1-one (Hyhexnon; Scheme 3).

The influence of amount of catalyst (**6**) on the oxidation of cyclohexene are shown in the Figure 5(a). At 70°C temperature, three different quantities of pre-swelled catalyst **6**, i.e. 0.035 g, 0.040 g and 0.045 g, were used while reacting a fixed amount of cyclohexene (0.414 g, 5 mmol) with 30% H_2O_2 (2.267 g, 20 mmol) in 10 ml of MeOH for 6 hr. As shown in Figure 5(a), by increasing the catalyst amount from 0.035 g to 0.040 g, the % conversion increases from 68.5% to 80.1%. Further increasing the catalyst amount from 0.040 g to 0.045 g, % conversion does not increase much in 6 hr. So, 0.040 g of catalyst was considered to be the best amount.

The impact of oxidant (30% H_2O_2) was studied by taking three different substrate to oxidant ratios, viz. 1:3, 1:4 and 1:5 for a fixed amount of pre-swelled catalyst **6** (0.040 g) and cyclohexene (0.414 g, 5 mmol) in 10 ml of MeOH at 70°C for 6 hr. Figure 5(b) presents the variation of % conversion with time. With increasing the substrate to oxidant ratio from 1:3 to 1:4, % conversion increased from 29.9% to 80.1%, while a 1:5 ratio showed marginal increment in the % conversion (85.2%). Hence, 1:4 substrate to oxidant ratio was considered to be optimum.

The influence of the amount of solvent is shown in Figure 5(c). To optimize the amount of solvent (MeOH), three different amounts of solvent were used while reacting 0.040 g of pre-swelled catalyst **6** with 0.414 g (5 mmol) of cyclohexene in the presence of 2.267 g (20 mmol) of 30% H_2O_2 at 70°C for 6 hr. Figure 5(c) indicates that with increasing the solvent volume from 5 ml to 10 ml and then 10 ml to 15 ml leads to the reduction in % conversion. This is because an increase in the

SCHEME 3 Oxidation products of cyclohexene catalyzed by **5–8** in the presence of hydrogen peroxide at 70°C in methanol

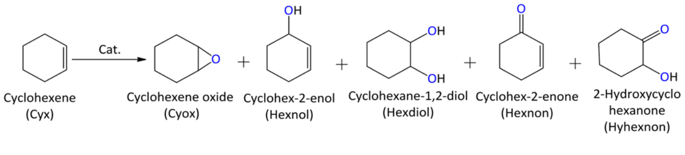

volume of solvent increases the inter-molecular distances and hence reduces the effective collision between the reactant molecules. As a result, 5 ml solvent gave 85.4% conversion, while 10 ml solvent exhibited 80.1% conversion. But on further increasing the volume, % conversion reduced rapidly and only 22.3% conversion was observed in 15 ml of MeOH. Withdrawing multiple numbers of samples from 5 ml of the reaction mixture can lead to a notable error in the result. Moreover, 10 ml solvent showed only 5% reduction in the % conversion, hence by minimizing the error without affecting the % conversion much, 10 ml solvent was chosen as an optimum solvent amount Figure 6(a)-(d).

Similarly, three different solvents, viz. MeOH, ACN and DMF, were used while keeping a fixed amount of pre-swelled catalyst **6** (0.040 g), cyclohexene (0.414 g, 5 mmol), 30% H_2O_2 (2.267 g, 20 mmol) in 10 ml of solvent at 70°C for 6 hr. The impact of solvent nature is shown in Figure 5(d). In methanol, oxidation of cyclohexene proceeds up to 80.1%, whereas DMF shows very close % conversion (78%), but acetonitrile exhibits only 69.7% conversion. This may be because of the fact that less polar solvents allow easy dispersion of reactants and product molecules compared with a high polar solvent like ACN. Hence, because of its cheap price, easy availability and high performance, methanol was considered as an optimum solvent. Finally, all the reaction conditions that were used to identify the optimized conditions in order to achieve the maximum oxidation of cyclohexene are listed in Table 5.

Serial No. 02 of Table 5 represents the optimized reaction conditions, which are: 0.040 g catalyst, 0.414 g (5 mmol) cyclohexene, 2.267 g (20 mmol) 30% H_2O_2, 10 ml of MeOH, 70°C and 6 hr of time. Only 8.4% conversion was observed while using TBHP (tert-butyl hydroperoxide) as an oxidant under the above-mentioned optimized reaction conditions, which unanimously supports the use of cheap and green oxidant hydrogen peroxide for the oxidation of cyclohexene. A blank reaction under the same optimized reaction conditions shows only 4.7% cyclohexene conversion. In optimized reaction conditions, cyclohex-2-enone (Hexnon) appears as a major product with 46.68% selectivity, whereas cyclohexene oxide (Cyox) shows only 18.59% selectivity. That means allylic oxidation predominates over epoxidation by catalyst **6**. The order of % selectivity of the products is: hexnon (46.68%) > hyhexnon (19.12%) > cyox (18.59%) > hexnol (9.92%) > hexdiol (5.67%). Catalytic activity of (**5**), (**7**) and (**8**) was also scrutinized against oxidation of cyclohexene under above-mentioned optimized reaction conditions, and is shown in Figure 7.

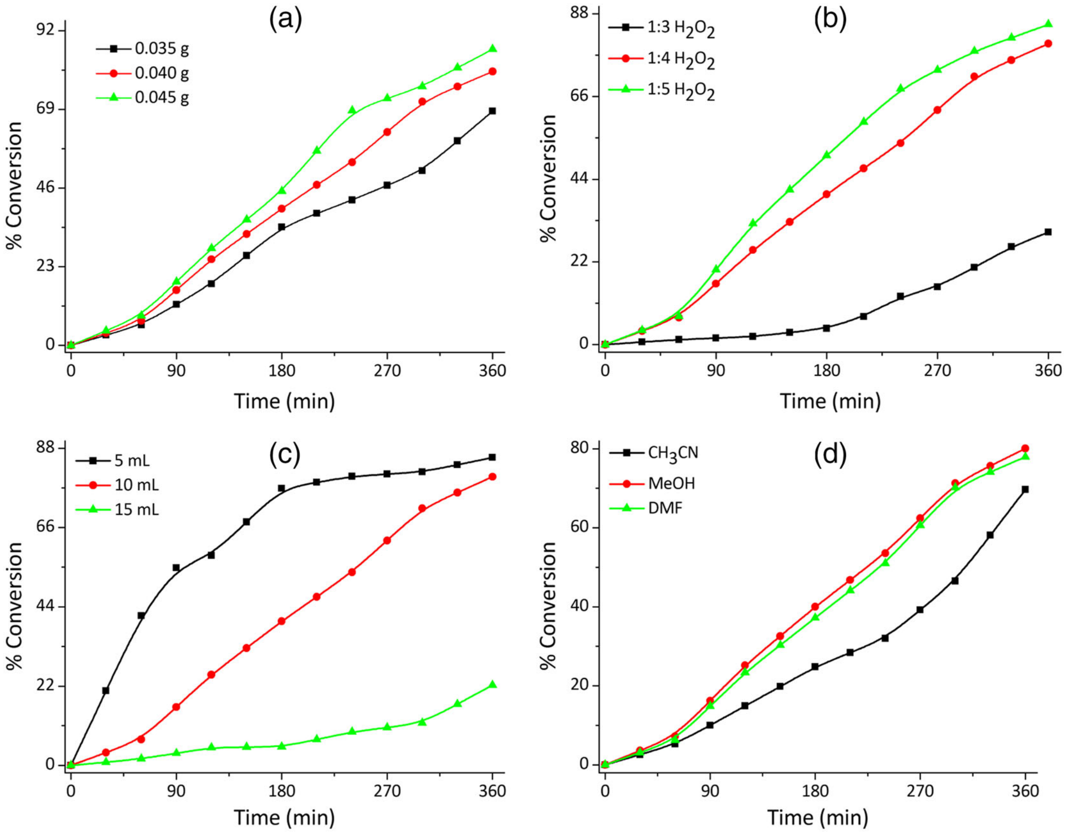

FIGURE 6 Catalytic oxidation of cyclohexene by hydrogen peroxide in the presence of **6** at 70°C. (a) Impact of amounts of catalyst; (b) effect of oxidant (H_2O_2) amounts; (c) influence of solvent (MeOH) amount; and (d) impact of nature of solvents

TABLE 5 Summarized results of all the reaction conditions applied to optimize the maximum oxidation of cyclohexene by catalyst **6** at 70°C

S.N.	Catalyst (mg)	Oxidant	Substrate: oxidant	Solvent	Solvent (ml)	% Conv.	TON	TOF (hr^{-1})
1	35	H_2O_2	1:4	MeOH	10	68.5	1.28×10^3	2.14×10^2
2	40	H_2O_2	1:4	MeOH	10	80.1	1.31×10^3	2.19×10^2
3	45	H_2O_2	1:4	MeOH	10	86.6	1.26×10^3	2.11×10^2
4	40	H_2O_2	1:3	MeOH	10	29.9	4.92×10^2	8.20×10^1
5	40	H_2O_2	1:5	MeOH	10	85.2	1.40×10^3	2.33×10^2
6	40	H_2O_2	1:4	MeOH	5	85.4	1.40×10^3	2.34×10^2
7	40	H_2O_2	1:4	MeOH	15	22.3	3.67×10^2	6.12×10^1
8	40	H_2O_2	1:4	ACN	10	69.7	1.14×10^3	1.91×10^2
9	40	H_2O_2	1:4	DMF	10	78	1.28×10^3	2.14×10^2
10	40	TBHP	1:4	MeOH	10	8.4	1.38×10^2	2.30×10^1

Reaction conditions: 0.040 g catalyst **6**, 0.414 g (5 mmol) cyclohexene, 2.267 g (20 mmol) 30% H_2O_2, 10 ml MeOH, 70°C and 6 hr.

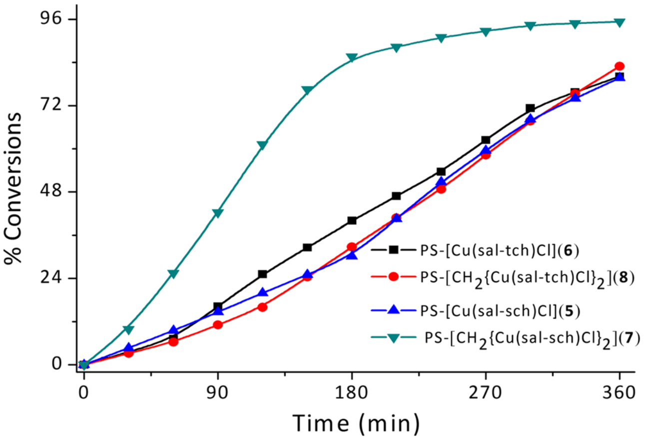

FIGURE 7 Catalytic oxidation of cyclohexene by PS-[Cu (sal-sch) Cl] (**5**), PS-[Cu (sal-tch)Cl] (**6**), PS-[CH_2{Cu (sal-sch)Cl}$_2$] (**7**) and PS-[CH_2{Cu (sal-tch)Cl}$_2$] (**8**) under optimized reaction conditions [which are 0.040 g catalyst **6**, 0.414 g (5 mmol); cyclohexene, 2.267 g (20 mmol); 30% H_2O_2; 10 ml of MeOH; 70°C and 6 hr]

With 79.7% conversion, the order of % selectivity of the products exhibited by catalyst **5** is hexnon (48.70%) > hyhexnon (15.07%) > hexnol (12.75%) > cyox (12.37%) > hexdiol (11.09%), whereas catalyst **7** shows a maximum of 95.3% conversion with the order of % selectivity of the products as hexnon (29.44%) > cyox (28.13%) > hexnol (19.78%) > hexdiol (18.12%) > hyhexnon (4.54%; Table 6). Catalyst **8** shows 82.9% conversion with the order of % selectivity of the products formed as hexnon (46.93%) > cyox (16.12%) > hexnol (13.26%) > hyhexnon (12.24%) > hexdiol (11.22%). Figure 7 indicates that among all the four catalysts, maximum oxidation (95.3%) of cyclohexene takes place in the presence of catalyst **7**, whereas **5** shows the least % conversion (79.7%).

However, considering the TOF values, catalyst **6** becomes the most efficient (TOF = 2.198×10^2 hr^{-1}), whereas with the TOF value of 7.674×10^1 hr^{-1}, **7** becomes the least efficient among the catalysts **1–8**. During the catalysis by neat complex, we used the same number of mmol of catalytic centers that is present in the optimized amount of supported catalyst. Based on the metal loading calculated from AAS data in catalysts **5–8**, actual mmol of metal centers were estimated and equivalent mmol of the respective neat catalyst were used in the reaction. Under the same optimized reaction conditions, neat complexes **1–4** caused only 62.3%, 72.8%, 80.3% and 71.35% conversions, respectively which is at least 10–15% less than what is actually observed for the polymer-anchored catalysts. Also, the TOF values of the neat complexes against the catalytic oxidation of cyclohexene are quite low in comparison to that of grafted catalysts (Table 6). That means grafting the neat complexes into the polymer matrix improves the % conversion as well as the efficiency significantly. Therefore, in spite of a large number of reports of transition metal-catalyzed cyclohexene oxidation, catalysts **5–8** stand strong among the available catalysts.[40] The above-mentioned optimized reaction conditions were extended towards the catalytic oxidation of *cis*-cyclooctene, styrene, 1-methyl cyclohexene and 1-hexene. At least four major products have been identified during the heterogeneous oxidation of *cis*-cyclooctene catalyzed by **5–8** in the presence of hydrogen peroxide.[41–47] All the oxidation products of *cis*-cyclooctene, i.e. cyclooctene oxide (Cytox), (Z)-cyclooct-2-enone (Cytnon), 2-hydroxycyclooctanone (Hycyt) and cyclooctane-1,2-diol (Cytdiol; Scheme 4) are well known and reported in the literature.

Under the optimized reaction conditions, time vs. % conversion plots for the oxidation of *cis*-cyclooctene by **5–8** are presented in Figure 8. From the figure, it is clear that a maximum of 79.4% conversion of *cis*-cyclooctene

TABLE 6 TOF values, % conversion and % selectivity of various oxidation products of cyclohexene by catalysts **1–8** under the optimized reaction conditions

S.N.	Cat.	% Conversion	TOF (hr^{-1})	% Selectivity of products Cyox	Hexnon	Hexnol	Hexdiol	Hyhexnon
1	**5**	79.7 (62.3)*	1.41×10^2 (1.10×10^2)*	12.37	48.70	12.75	11.09	15.07
2	**6**	80.1 (72.8)*	2.19×10^2 (2.01×10^2)*	18.59	46.68	9.92	5.67	19.12
3	**7**	95.3 (80.3)*	7.67×10^1 (1.03×10^1)*	28.13	29.44	19.78	18.12	4.54
4	**8**	82.9 (71.3)*	1.05×10^2 (1.63×10^1)*	16.12	46.93	13.26	11.22	12.24

*Respective neat complexes.Reaction conditions: 0.040 g catalyst, 0.414 g (5 mmol) cyclohexene, 2.267 g (20 mmol) 30% H_2O_2, 10 ml MeOH, 70°C and 6 hr.

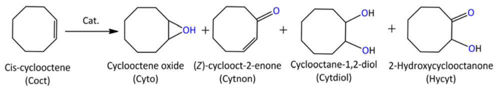

SCHEME 4 Oxidation products of *cis*-cyclooctene in the presence of catalysts **5–8** and hydrogen peroxide

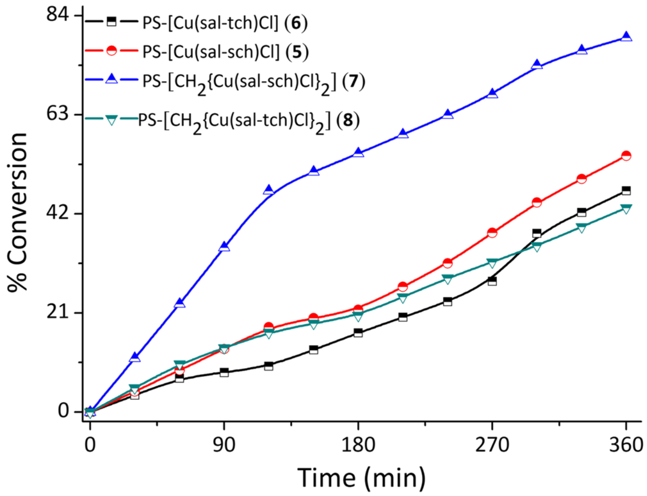

FIGURE 8 The oxidation of *cis*-cyclooctene by the catalysts PS-[Cu (sal-sch)Cl] (**5**), PS-[Cu (sal-tch)Cl] (**6**), PS-[CH_2{Cu (sal-sch) Cl}$_2$] (**7**) and PS-[CH_2{Cu (sal-tch)Cl}$_2$] (**8**) under optimized reaction conditions

was achieved by catalyst **7**, whereas catalysts **5**, **6** and **8** showed 54.3%, 46.9% and 43.3% conversion, respectively. In terms of efficiency, the TOF order is: **6** (1.289×10^2 hr^{-1}) > **5** (9.625×10^1 hr^{-1}) > **7** (6.393×10^1 hr^{-1}) > **8** (5.531×10^1 hr^{-1}).

Epoxidation gets preference over allylic oxidation during the oxidation of *cis*-cyclooctene by the anchored catalysts **5–8**. Only 4.91%, 5.73%, 3.90% and 5.20% selectively of allylic oxidation was observed in the presence of the catalysts **5–8**, respectively. Out of the epoxidation products (Cyto, Cytnon, Cytdiol and Hycyt), cyclooctene epoxide (Cyto) with approximately 45–50% selectivity appears as a major product in all cases. The detailed % selectivity of oxidized products of *cis*-cyclooctene is shown in Table 7.

Under the same optimized reaction conditions, neat catalysts **1–4** exhibit 47.3%, 36.4%, 62.3% and 37.3% conversion, respectively. Data presented in Table 7 reveal that improvement in the efficiency, as well as % conversion, is achieved by heterogenization of the homogeneous catalysts **1–4**. Controlled reaction without catalyst shows only 1.80% conversion. With respect to the recently accessible literature,[41–45] catalysts **5–8** appear stronger candidates for heterogeneous oxidation of *cis*-cyclooctene. Likewise, at least six major products, styrene oxide (SO), benzaldehyde (Bza), benzoic acid (Bzac), 2-phenylacetaldehyde (Pha), 2-hydroxy-1-phenylethanone (Hyphon) and acetophenone (Acph) have been identified (Scheme 5) during the oxidation of styrene catalyzed by PS-[Cu (sal-sch)Cl] (**5**), PS-[Cu (sal-tch)Cl] (**6**), PS-[CH_2{Cu (sal-sch)Cl}$_2$] (**7**) and PS-[CH_2{Cu (sal-tch) Cl}$_2$] (**8**). Identification of all the oxidized products was confirmed by GC–MS, which is also widely reported in the literature.[48–54]

The impact of various catalysts has been depicted in Figure 9. Among the catalysts **5–8**, catalyst **7** was the best one to attain a maximum of 54.7% conversion within 6 hr of time with a TOF value of 4.40×10^1 hr^{-1}, while 22.9%, 29.5% and 44.8% conversion were attained by **5**, **6** and **8**, respectively. Moreover, neat complexes **1–4** showed 17.1% (TOF = 3.033×10^1 hr^{-1}), 20.2% (TOF = 5.583×10^1 hr^{-1}), 45.8% (TOF = 5.98 hr^{-1}) and 31.2% (TOF = 7.33 hr^{-1}) conversion, respectively, which indicates the amplification of the reactivity and efficiency by heterogenization of the neat complexes into the polymer chain. Blank reaction under optimized reaction conditions showed only 2.3% conversion.

Details of % selectivity of oxidation products of styrene are given in Table S6. Among all the epoxidation products, benzaldehyde appeared as a major product during the catalytic oxidation of styrene in the presence of catalysts **1–8**. Although oxidation of styrene has been reported in a number of research articles, still catalysts **5–8** can be placed easily amongst the top catalysts owing to their excellent catalytic efficiency, versatility, stability, feasible synthesis and heterogeneous nature.[55]

TABLE 7 Selectivity of the oxidized products of *cis*-cyclooctene under optimized reaction conditions

S.N.	Catalyst	% Conversion	TOF (hr^{-1})	% Selectivity of products (Cyto)	(Cytnon)	(Cytdiol)	(Hycyt)
1	**5**	54.3 (47.3)*	9.62×10^1 (8.38×10^1)*	44.70	4.91	28.10	22.26
2	**6**	46.9 (36.4)*	1.28×10^2 (1.00×10^2)*	45.15	5.73	30.20	18.89
3	**7**	79.4 (62.3)*	6.39×10^1 (8.00)*	48.00	3.90	29.18	18.91
4	**8**	43.3 (37.3)*	5.53×10^1 (8.53)*	57.84	5.20	23.22	13.67

*Respective neat catalysts.

Reaction conditions: 0.040 g catalyst, 0.414 g (5 mmol) cis-cyclooctene, 2.267 g (20 mmol) 30% H_2O_2, 10 ml MeOH, 70°C and 6 hr.

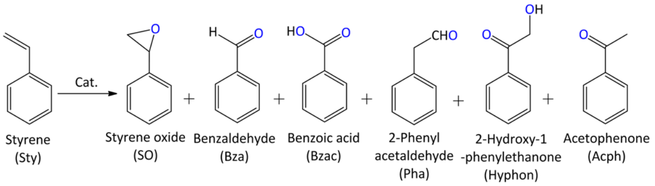

SCHEME 5 Oxidation products of styrene under optimized reaction conditions catalyzed by the catalysts **5–8**

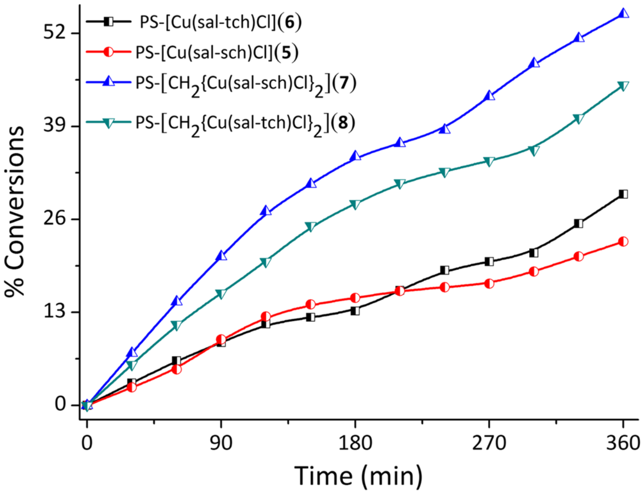

FIGURE 9 The oxidation of styrene by the catalysts PS-[Cu (sal-sch)Cl] (**5**), PS-[Cu (sal-tch)Cl] (**6**), PS-[CH_2{Cu (sal-sch)Cl}$_2$] (**7**) and PS-[CH_2{Cu (sal-tch)Cl}$_2$] (**8**) under optimized reaction conditions

Catalytic oxidation of 1-methyl cyclohexene in the presence of hydrogen peroxide results in epoxidation, allylic oxidation as well as oxidative cleavage simultaneously. At least six oxidation products: 1-methylcyclohexaneepoxide (Mcyo), 3-methylcyclohex-2-enone (Mcxnon), 2-methylcyclohex-2-enol (Mcxnol), 1-methylcyclohexanol (Mcynol), 1-methylcyclohexane-1,2-diol (Mcdiol) and (E)-hept-3-en-2-one (Hpon) along with a number of unidentified products were produced during the course of the oxidation by PS-[Cu (sal-sch)Cl](**5**), PS-[Cu (sal-tch)Cl](**6**), PS-[CH_2{Cu (sal-sch)Cl}$_2$](**7**) and PS-[CH_2{Cu (sal-tch)Cl}$_2$](**8**) under optimized reaction conditions. These are the usual oxidation products of 1-methyl cyclohexene, and are also available in the literature (Scheme 6).[7c,56,57]

Time vs. % conversion plots for the catalytic oxidation of 1-methyl cyclohexene are displayed in Figure 10. With a TOF value of 1.331×10^2 hr^{-1} catalyst **5** shows 75.1% conversion, and with a TOF value of 2.441×10^2 hr^{-1} catalyst **6** presents 89.0% conversion. Catalyst **7** exhibits 76.7% conversion with a TOF value of 6.180×10^1 hr^{-1} and catalyst **8** shows 62.2% conversion with a TOF value of 7.945×10^1 hr^{-1} (Table S7). Corresponding neat complexes show only 65.3%, 78.4%, 68.9% and 55.1% conversions, respectively. Observed TOF values of complexes **7** and **8** are significantly lower in comparison to their anchored ones, indicating improvement in their efficiency along with the overall % conversion by heterogenization. Detailed selectivity of the oxidation products of 1-methylcyclohexene along with the % conversion and TOF values are shown in Table S7. All the supported catalysts **5–8** efficiently catalyzed 1-methylcyclohexene oxidation. In this oxidation, epoxidation gets preference over allylic oxidation and oxidative cleavage. Selectivities of the oxidation products for **5** and **6** are comparable and follow the order: (Mcdiol) > (Hpon) > (Mcyo) > (-Mcxnon) > (Mcynol) > (Mcxnol), whereas **7** and **8** display the following order: (Mcdiol) > (Hpon) > (Mcxnon) > (Mcynol) > (Mcyo) > (Mcxnol).

Controlled reaction under the same optimized conditions without catalyst gave 5.21% conversion. Catalytic oxidation of 1-methylcyclohexene in the presence of hydrogen peroxide is very limited.[56,57] Hence, by considering the current availability of the heterogeneous catalysts for the oxidation of 1-methylcyclohexene, reported catalysts **5–8** appear to be the most suitable option due to their high % conversion and TOF values. Finally, oxidation of 1-hexene by PS-[Cu (sal-sch)Cl] (**5**), PS-[Cu (sal-tch)Cl] (**6**), PS-[CH_2{Cu (sal-sch)Cl}$_2$] (**7**) and

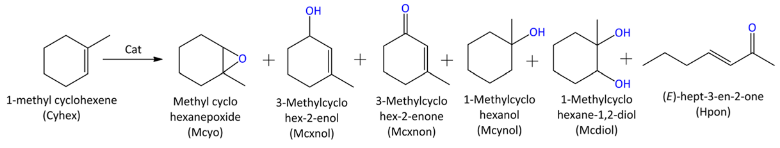

SCHEME 6 Oxidation products of 1-methyl cyclohexene catalyzed by the catalysts **5–8**

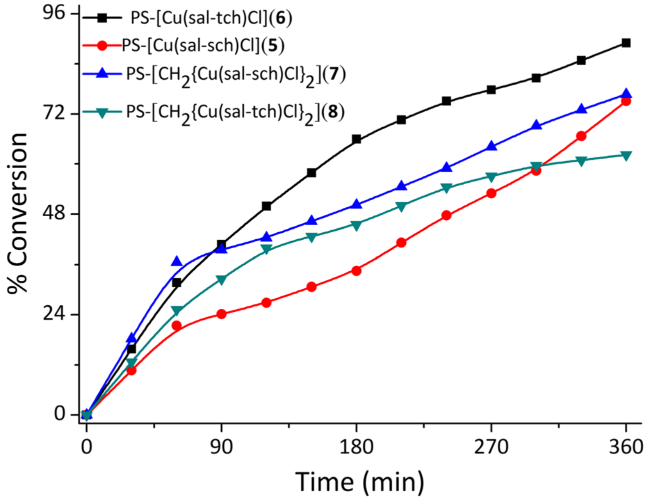

FIGURE 10 Time vs. % conversion plots for the oxidation of 1-methyl cyclohexene by the catalysts PS-[Cu (sal-sch)Cl] (**5**), PS-[Cu (sal-tch)Cl] (**6**), PS-[CH_2{Cu (sal-sch)Cl}$_2$] (**7**) and PS-[CH_2{Cu (sal-tch)Cl}$_2$] (**8**)

PS-[CH_2{Cu (sal-tch)Cl}$_2$] (**8**) was examined, and their corresponding time vs. % conversion plots are presented in Figure 11.

Under optimized reaction conditions, oxidation of 1-hexene affords three products, formic acid (Fa), pentanal (Pan) and Hexane epoxide (Hexo; Scheme 7), as expected from the literature. However, oxidation of 1-hexene is not very common in the literature.[58–61]

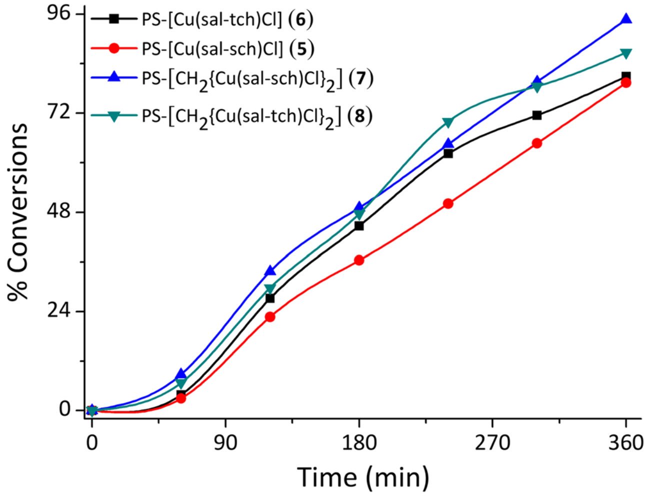

FIGURE 11 Oxidation of 1-hexene by the catalysts PS-[Cu (sal-sch)Cl] (**5**), PS-[Cu (sal-tch)Cl] (**6**), PS-[CH_2{Cu (sal-sch)Cl}$_2$] (**7**) and PS-[CH_2{Cu (sal-tch)Cl}$_2$] (**8**)

With a TOF value of 1.43×10^2 hr^{-1} catalyst **5** shows 80.9% conversion, and with a TOF value of 2.18×10^2 hr^{-1} catalyst **6** displays almost identical (79.4%) conversion to that of catalyst **5**. However, **7** shows 94.7% conversion with a TOF value of 7.62×10^1 hr^{-1} and **8** attained a TOF value of 1.10×10^2 hr^{-1} with 86.7% conversion. Corresponding neat complexes **1–4** displayed 67.7%, 64.2%, 82.3% and 70.2% conversions, respectively. Also, the efficiencies achieved by these catalysts are much less in comparison to the supported complexes, which is revealed by the lower TOF values achieved by the neat complexes, especially for catalysts **7** and **8** (Table S8). Detailed % conversion, TOF and % selectivity for the oxidation of 1–hexene are listed in Table S8. Among the three oxidation products, formic acid (Fa) was found as a major product, and the selectivity varies in the order: formic acid > pentanal > hexane epoxide. It is evident from Table S8 that oxidation of 1-hexene mainly proceeds through oxidative cleavage rather than epoxidation or allylic oxidation in the presence of supported catalysts **5–8**. A limited number of heterogeneous catalysts are reported in the literature for the oxidation of 1-hexene in the presence of hydrogen peroxide.[59,62] Thus, **5–8** can be considered as a potential addition for the oxidation of 1-hexene with respect to the currently available catalysts.[60–64] A controlled reaction under the optimized conditions without catalyst showed only 3.98% conversion.

All the alkenes are effectively oxidized by the reported catalysts, except styrene. The relatively low reactivity of styrene in comparison to the other non-aromatic alkenes (cyclohexene, *cis*-cyclooctene, 1-methyl cyclohexene and 1-hexene) towards the oxidation can be explained by the fact that conjugation of the π-electron cloud of the vinyl group with the phenyl ring makes it less available for the oxidation reaction. However, the supported catalysts are more effective and more efficient in all cases in comparison to their homogeneous counterparts.

3.10 | Recyclability test of the catalysts

Reusability of the polymer-supported catalysts **5–8** was tested and presented in Figure S18. After completing the reaction, supported catalysts **5–8** were filtered off, washed with methanol and dried in an oven at 120°C for 24 hr. FT-IR spectra of the recycled catalysts are shown in Figure S19, which displays all the important stretching

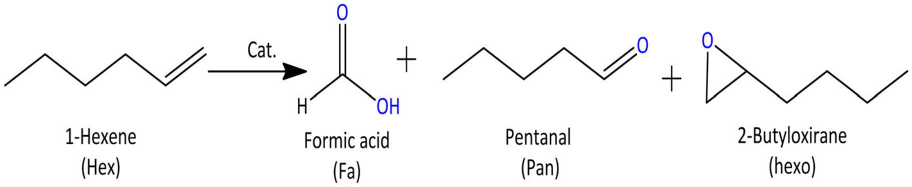

SCHEME 7 Oxidation products of 1-hexene

bands comparable to that of fresh ones suggesting the existence of a similar molecular structure in the polymer matrix. Comparable UV–Vis spectral patterns (Figure S6) of the recycled catalysts with the fresh ones also support the FT-IR analysis. SEM analysis of the used catalysts (Figure S20) displays the unchanged surface morphology even after the catalytic reaction. EDX analysis (Figure S21) identifies all the elemental signals similar to that of the fresh catalysts, suggesting that the physical and structural nature remains the same after the catalytic reactions, although AAS data (listed in Table S9) suggest elimination of physically adsorbed complexes along with the leaching of a small fraction of copper complexes from the polymer beads during the course of the catalytic reactions, which can be evident from small reduction in the % conversion in the 2nd and 3rd cycles (Figure S18) of the catalytic processes. In all the cases, % conversion was found to be within the limits of experimental error, which supports the heterogeneous nature of the supported catalysts. Thus, catalysts **5–8** can be accepted as efficient heterogenized catalysts for the oxidation of alkenes.

3.11 | Mechanism

A number of reaction pathways of alkene oxidation catalyzed by transition metals in the presence of H_2O_2 are discussed[38,65–70] in the literature. Generally, the reaction mechanism suggested by Mimoun *et al.* in 1970 and the mechanism suggested by Sharpless *et al.* in 1972 were contested. Mimoun proposed a multi-step mechanism,[67] which proceeds with the formation of metal olefin complexes, followed by the generation of a five-member metallacycle intermediate. On the other hand, Sharpless proposed a concerted reaction pathway,[69] involving the reaction of an olefin with one of the peroxo oxygens and forming a spiro-like intermediate. In the whole catalytic cycle, there is no direct contact between the transition metal and the olefin. Later, theoretical calculations[71] also suggested that the oxidation of alkenes catalyzed by transition metals in the presence of hydrogen peroxide is more likely to proceed through the Sharpless-type pathway. From the electronic spectroscopic studies in combination with LC–MS and EPR spectroscopy, we have proposed a reaction pathway (considering the Sharpless-type reaction mechanism) for the oxidation of alkenes in the presence of hydrogen peroxide using the catalysts reported in the present study, and shown in Scheme 8.

Aqueous H_2O_2 was added in DMF solution of a representative catalyst [Cu (Hsal-sch)Cl] (**1**), and the change in spectral bands was recorded by UV–Vis spectrometer (Figure 12). The disappearance of 724 nm absorption band (*d-d* transition) by the introduction of hydrogen peroxide indicates the conversion of Cu^{II} center into Cu^{III} in solution, and the formation of copper peroxo or hydroperoxo species is suggested. In the presence of hydrogen peroxide, three peroxo species, namely side-on Cu^{III}–(μ-η^2-peroxido)–Cu^{III}, bis (μ-oxido–Cu^{III}), and Cu^{III}–O–O–H, were reported in the course of the catalytic reaction.[72–74] Because of the monomeric nature of the catalyst **1** (**A**), two types of peroxo species can be expected, i.e. copper hydroperoxo [Cu^{III} (sal-sch)-O-O-H] (**A$_1$**) and copper peroxo [$Cu^{III}(O)_2$(sal-sch)] (**A$_2$**; Figure 13).

The theoretical calculation shows that formation of the hydroperoxo species (**A$_1$**) is energetically more favorable over the peroxo species (**A$_2$**). The change in Gibbs free energy (Δ*G*) during the generation of hydroperoxo (**A$_1$**) and peroxo (**A$_2$**) species from [Cu^{II} (Hsal-sch)Cl] (**1**) (**A**) is 3.3596×10^2 kcal/mole and 7.2731×10^2 kcal/mole,

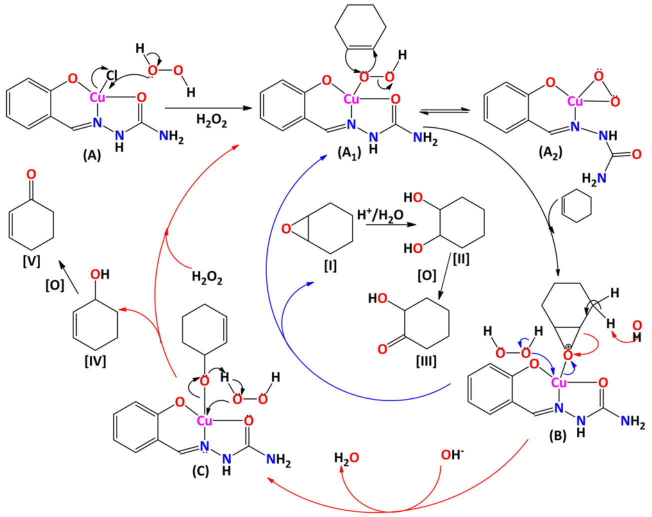

SCHEME 8 Proposed reaction mechanism for oxidation of alkenes catalyzed by the synthesized copper complexes in the presence of H_2O_2

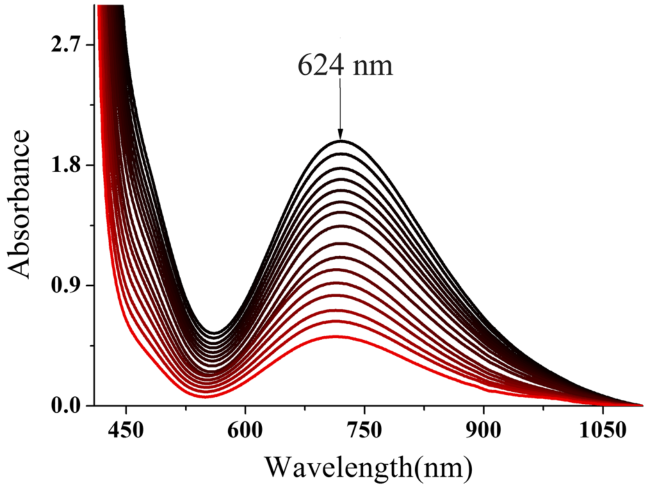

FIGURE 12 Change in UV–Vis spectra of [Cu (Hsal-sch)Cl] (**1**), observed during titration with 30% aqueous H_2O_2. The spectra were recorded after gradual addition of three-drop portions of H_2O_2 [10 ml, 7.40×10^{-1} (M) H_2O_2 in DMF] in 15 ml of 2.17×10^{-2} M solution of [Cu (Hsal-sch)Cl] (**1**) in DMF

respectively, while ΔE, i.e. reaction energy for the formation of $\mathbf{A_2}$, is 7.492969391×10^2 kcal/mole and the formation energy of ($\mathbf{A_1}$) is only 3.460654401×10^2 kcal/mole. Moreover, the change in Gibb's free energy for the conversion of ($\mathbf{A_2}$) from ($\mathbf{A_1}$) is also negative ($\Delta G = -3.9131 \times 10^2$ kcal/mole). Therefore, the hydroperoxo species ($\mathbf{A_1}$) present in the reaction mixture predominates over the peroxo ($\mathbf{A_2}$) species during the course of the catalytic reaction. The LC–MS spectra display an m/z signal of (M^+) = 274.1 (Figure S22) while monitoring the hydrogen peroxide mixed methanolic solution of complex **1**, confirming the formation of [Cu^{III} (sal-sch)-O-O-H] ($\mathbf{A_1}$) in the catalytic reaction. Further, metal oxidation state in the peroxo form ($\mathbf{A_1}$) was confirmed by monitoring changes in the EPR spectra during titration of the methanolic solution of [Cu^{II} (sal-sch)Cl]) (**1**) with dilute hydrogen peroxide solution (Figure S23). The gradual addition of dilute hydrogen peroxide solution to the methanolic solution of **1** causes the disappearance of the characteristic EPR spectral pattern of Cu^{II}, which suggests the formation of EPR silent Cu^{III} species in solution. All the above findings conclude the formation of active species [Cu^{III} (sal-sch)-O-O-H] ($\mathbf{A_1}$) in solution during the catalytic reaction.

In the second step, the hydroperoxo species ($\mathbf{A_1}$) interacts with cyclohexene through one of the peroxo oxygens and produces the intermediate (**B**) via a spiro-like transition state.

Regeneration of the active catalyst ($\mathbf{A_1}$) in solution from the intermediate (**B**) proceeds through two paths. In the first pathway (marked by the blue arrow), cyclohexanone (**I**) detaches from the copper center of intermediate (**B**) while a subsequent attack by

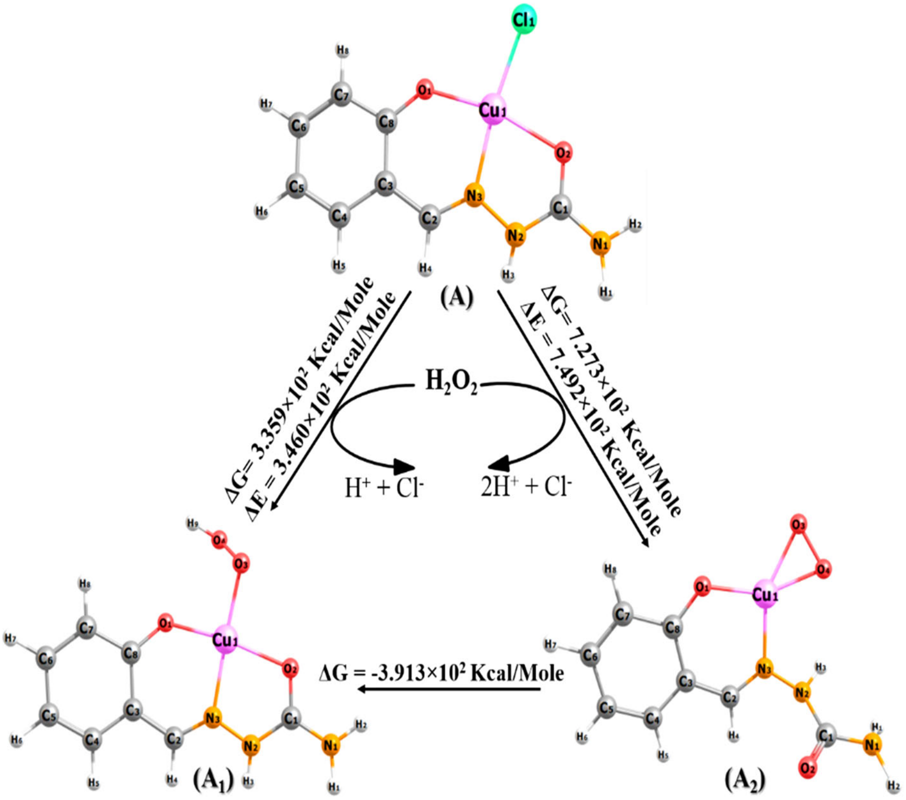

FIGURE 13 Formation of peroxo species by the reaction of ([Cu (sal-sch)Cl]) (**1**) with H_2O_2

hydrogen peroxide reproduces the active species (**A_1**) in solution. Hydrolysis of cyclohexene oxide (**I**) produces cyclohexane-1,2-diol (**II**), which by partial oxidation generates 2-hydroxycyclohexan-1-one (hyhexnon, **III**). The second pathway begins with the abstraction of β-hydrogen of cyclohexene oxide ring and gives rise to the intermediate (**C**), which further reacts with hydrogen peroxide to provide cyclohex-2-enol (**IV**) and regenerates the active peroxo species (**A_1**) in the solution. Further oxidation of cyclohex-2-enol (**IV**) produces cyclohex-2-enone (**V**).

Roughly similar product distribution can be observed during the catalytic oxidation of cyclohexene, 1-methyl cyclohexene and styrene, except for cis-cyclooctene. During the catalytic oxidation of *cis*-cyclooctene using the catalysts **5–8**, epoxidation products appear as major products along with a small percentage of allylic oxidation. Thus, regeneration of active catalyst during the catalytic oxidation of *cis*-cyclooctene proceeds preferentially through path 1 and hence favors the epoxidation over allylic oxidation.

4 | CONCLUSIONS

Four Cu^{II} complexes [Cu (sal-sch)Cl] (**1**), [Cu (sal-tch)Cl] (**2**), [CH_2{Cu (sal-sch)Cl}$_2$] (**3**) and [CH_2{Cu (sal-tch)Cl}$_2$] (**4**) were synthesized successfully by reacting $CuCl_2{\cdot}2H_2O$ with the ligands [Hsal-sch] (**I**), [Hsal-tch] (**II**), [H_2bissal-sch] (**III**) and [H_2bissal-tch] (**IV**). Complexes **1–4** were grafted into the polymeric matrix of Merrifield resin. All the compounds are characterized in solution and in solid state through a number of analytical and spectroscopic techniques. Supported catalysts **5–8** efficiently catalyzed the oxidation of cyclohexene, *cis*-cyclooctene, styrene, 1-methyl cyclohexene and 1-hexene. Supported catalysts **5–8** favor allylic oxidation over epoxidation during the cyclohexene oxidation, whereas epoxidation gets preference over allylic oxidation during the oxidation of *cis*-cyclooctene. Styrene undergoes epoxidation followed by oxidative cleavage, 1-methyl cyclohexene inclines towards allylic oxidation, while oxidation of 1-hexene proceeds mainly with the oxidative cleavage of C=C. In spite of a small amount of metal leaching during the catalytic cycles, catalysts **5–8** are quite unique and can be an effective choice for the oxidation of alkenes. Corresponding neat complexes also show competitive efficiency and activity, but easy separation, higher thermal stability and uncomplicated synthesis makes the supported catalysts a better option for the catalytic oxidation of alkenes. Formation of hydroperoxo species ([Cu^{III} (sal-sch)-O-O-H]) (**A_1**) was suggested during the course of alkene oxidation and established through UV–Vis, LC–MS and EPR studies.

ACKNOWLEDGEMENTS

C.H. thanks the Science and Engineering Research Board (SERB), Department of Science and Technology (DST), the Government of India, New Delhi, for financial support (grant no. SB/EMEQ-055/2014) of the work. V.K.M. acknowledges the SERB, DST, New Delhi for a fellowship. A.M., N.K. and P.K. are thankful to IIT (ISM) Dhanbad for fellowship. C.H. is very thankful to Prof. Delia Haynes, Department of Chemistry and Polymer Science, Stellenbosch University, South Africa for providing EPR facility. The authors would like to thank Dr G.C. Nayak, Department of Applied Chemistry, IIT (ISM) Dhanbad, India for SEM and EDX analysis. The authors would like to thank SAIF Mumbai for TGA/DTA analysis. The authors acknowledge SAIF Punjab University for NMR and ESI-MS data. The authors also acknowledge CFR IIT (ISM) Dhanbad for providing AFM analysis. GC used in this study was procured from the grant given by Science and Engineering Research Board (SERB), Department of Science and Technology (DST), grant no. SB/FT/CS-027/2014), Government of India, New Delhi, India, to C.H.

Conflict of interest

There are no conflicts of interest to declare.

ORCID

Chanchal Haldar https://orcid.org/0000-0003-4642-7918

REFERENCES

[1] (a)T. Bunchuay, R. Ketkaew, P. Chotmongkolsap, T. Chutimasakul, J. Kanarat, Y. Tantirungrotechai, J. Tantirungrotechai, *Cat. Sci. Technol.* **2017**, *7*, 6069. (b)W. J. Ang, Y. Lam, *Org. Biomol. Chem.* **2015**, *13*, 1048. (c)M. M. Hossain, S.-G. Shyu, *Tetrahedron* **2014**, *70*, 251. (d)Z. P. Pai, N. V. Selivanova, P. V. Oleneva, P. V. Berdnikova, A. M. Beskopyl'nyi, *Cat. Com.* **2017**, *88*, 45.

[2] C. Weerakkody, S. Biswas, W. Song, J. He, N. Wasalathanthri, S. Dissanayake, D. A. Kriz, B. Dutta, S. L. Suib, *Appl. Catal. B* **2018**, *221*, 681.

[3] K. Parida, K. G. Mishra, S. K. Dash, *Ind. Eng. Chem. Res.* **2012**, *51*, 2235.

[4] (a) K. Koike, G. Inoue, T. Fukuda, *J. Chem. Eng. Jpn.* **1999**, *32*, 295. (b) S. B. Dorofeev, A. V. Eletskii, B. M. Smimov, *Sov. Phys. Dokl.* **1981**, *26*, 318. (c) R. A. Ogle, J. L. Schumacher, *Process Saf. Prog.* **1998**, *17*, 127.

[5] (a)K. Kaneda, S. Haruna, T. Imanaka, K. Kawamoto, *J. Chem. Soc. Chem. Commun.* **1990**, 1467. (b)B. R. Travis, R. S. Narayan, B. Borhan, *J. Am. Chem. Soc.* **2002**, *124*, 3824. c W. Yu, Y. Mei, Y. Kang, Z. Hua, Z. Jin, *Org. Lett.* **2004**, *6*, 3217. (d) D. C. Whitehead, B. R. Travis, B. Borhan, *Tetrahedron Lett.* **2006**, *47*, 3797. (e)K. C. Nicolaou, V. A. Adsool, C. R. H. Hale, *Org. Lett.* **2010**,

12, 1552. (f)R. D. Arasasingham, G.-X. He, T. C. Bruice, *J. Am. Chem. Soc.* **1993**, *115*, 7985. (g)K. Sato, L. Aoki, R. Noyori, *Science* **1998**, *281*, 1646. (h)W. A. Hermann, T. Weskamp, J. P. Zoller, R. W. Fischer, *J. Mol. Catal. A Chem.* **2000**, *153*, 49. (i) A. Wang, H. Jiang, *J. Org. Chem.* **2010**, *75*, 2321. (j)T. M. Shaikh, F.-E. Hong, *Adv. Synth. Catal.* **2011**, *353*, 1491. (k)S. Ma, J. Liu, S. Li, B. Chen, J. Cheng, J. Kuang, Y. Liu, B. Wan, Y. Wang, J. Ye, Q. Yu, W. Yuan, S. Yu, *Adv. Synth. Catal.* **2011**, *353*, 1005. (l)D. Xing, B. Guan, G. Cai, Z. Fang, L. Yang, Z. Shi, *Org. Lett.* **2006**, *8*, 693.

[6] (a)T. Dohi, N. Takenaga, A. Goto, H. Fujioka, Y. Kita, *J. Org. Chem.* **2008**, *73*, 7365. (b)M. Ochiai, T. Ito, H. Takahashi, A. Nakanishi, M. Toyonari, T. Sueda, S. Goto, M. Shiro, *J. Am. Chem. Soc.* **1996**, *118*, 7716. (c)Y. Zhao, Y.-Y. Yeung, *Org. Lett.* **2010**, *12*, 2128.

[7] (a) M. A. Fousteric, A. I. Koutsourea, S. S. Nikolaropoulos, A. Riahi, J. Muzart, *J. Mol. Catal.* **2006**, *250*, 70. (b)J. Q. Yu, E. J. Corey, *Org. Lett.* **2002**, *4*, 2727. (c)A. J. Catino, R. E. Forslund, M. P. Doyle, *J. Am. Chem. Soc.* **2004**, *126*, 13 622. (d)H. Peng, A. Lin, Y. Zhang, H. Jiang, J. Zhou, Y. Cheng, C. Zhu, H. Hu, *ACS Catal.* **2012**, *2*, 163. (e)Y. Li, T. B. Lee, T. Wang, A. V. Gamble, A. E. V. Gorden, *J. Org. Chem.* **2012**, *77*, 4628. (f)M. JuradoGonzalez, A. C. Sullivan, J. R. H. Wilson, *Tetrahedron Lett.* **2003**, *44*, 4283. (g)T. K. M. Shing, Y.-Y. Yeung, P. L. Su, *Org. Lett.* **2002**, *4*, 3149. (h)J. A. R. Salvador, J. H. Clark, *Chem. Commun.* **2001**, *6*, 33. (i)J. A. S. Coelho, A. F. Trindade, R. Wanke, B. G. M. Rocha, L. F. Veiros, P. M. P. Gois, A. J. L. Pombeiro, C. A. M. Afonso, *Eur. J. Org. Chem.* **2013**, *2013*, 1471. (j)J.-B. Xia, K. W. Cormier, C. Chen, *Chem. Sci.* **2012**, *3*, 2240. (k)C. Zou, Z. Zhang, X. Xu, Q. Gong, J. Li, C.-D. Wu, *J. Am. Chem. Soc.* **2012**, *134*, 87. (l)X. L. Yang, M.-H. Xie, C. Zou, Y. He, B. Chen, M. O'Keeffe, C.-D. Wu, *J. Am. Chem. Soc.* **2012**, *134*, 10 638. (m)C. S. Yi, K.-H. Kwon, D. W. Lee, *Org. Lett.* **2009**, *11*, 1567. (n)T. Nagano, S. Kobayashi, *Chem. Lett.* **2008**, *37*, 1042.

[8] M. W. Wang, C. H. Lin, T. Y. Juang, *Macromolecules* **2013**, *46*, 8853.

[9] M. J. Frisch, *GAUSSIAN 09, Rev. D.01*, Gaussian, Wallingford, CT **2009**.

[10] R. D. Dennington II, T. A. Keith, J. M. Millam, GaussView 5.0, Wallingford, CT, **2009**.

[11] A. D. Becke, *J. Chem. Phys.* **1993**, *98*, 5648.

[12] C. Lee, W. Yang, R. G. Parr, *Phys. Rev. B* **1988**, *37*, 785.

[13] B. D. Becke, *Phys. Rev. B* **1988**, *38*, 3098.

[14] (a)J. Patole, S. Dutta, S. Padhye, E. Sinn, *Inorg. Chim. Acta* **2001**, *318*, 207. (b)N. M. H. Salem, A. R. Rashad, L. E. Sayed, S. Foro, W. Haase, M. F. Iskander, *Inorg. Chim. Acta* **2015**, *432*, 231.

[15] S. Tangestaninejad, M. H. Habibi, V. Mirkhani, M. Moghadam, G. Grivani, *J. Mol. Catal. A Chem.* **2006**, *255*, 249.

[16] V. K. Singh, A. Maurya, N. Kesharwani, P. Kachhap, S. Kumari, A. K. Mahato, V. K. Mishra, C. Haldar, *J. Coord. Chem.* **2018**, *71*, 520.

[17] M. R. Maurya, P. Saini, C. Haldar, F. Avecilla, *Polyhedron* **2012**, *31*, 710.

[18] T. Abe, T. Kuribayashi, M. Nakamura, *Eur. J. Mineral.* **2017**, *29*(6), 949.

[19] M. R. Maurya, C. Haldar, A. A. Khan, A. Azam, A. Salahuddin, A. Kumar, J. C. Pessoa, *Eur. J. Inorg. Chem.* **2012**, *2012*, 2560.

[20] M. R. Maurya, C. Haldar, A. Kumar, M. L. Kuznetsov, F. Avecilla, J. C. Pessoa, *Dalton Trans.* **2013**, *42*, 11941.

[21] T. Sun, Q. Niu, Z. Guo, T. Li, *Tetrahedron Lett.* **2017**, *58*(3), 252.

[22] S. Kumari, A. K. Mahato, A. Maurya, V. K. Singh, N. Kesharwani, P. Kachhap, I. O. Koshevoy, C. Haldar, *New J. Chem.* **2017**, *41*, 13 625.

[23] E. Faggi, R. Gavara, M. Bolte, L. Fajarí, L. Juliá, L. Rodríguez, I. Alfonso, *Dalton Trans.* **2015**, *44*, 12 700.

[24] M. Lavanya, M. Jagadeesh, J. Haribabu, R. Karvembu, H. K. Rashmi, P. Uma Maheswari, A. V. R. Devi, *Inorg. Chim. Acta* **2018**, *469*, 76.

[25] A. J. Amoroso, M. W. Burrows, S. J. Coles, R. Haigh, R. D. Farley, M. B. Hursthouse, M. Jones, K. M. A. Malik, D. M. Murphy, *Dalton Trans.* **2008**, 506.

[26] T. H. Bennur, D. Srinivas, P. Ratnasamy, *Micropor. Mesopor. Mater.* **2001**, *48*, 111.

[27] C. G. Zhan, J. A. Nichols, D. A. Dixon, *J. Phys. Chem. A* **2003**, *107*, 20.

[28] S. J. J. Titinchi, G. V. Willingh, H. S. Abbo, R. Prasad, *Cat. Sci. Technol.* **2015**, *5*, 325.

[29] M. R. Maurya, A. Arya, U. Kumar, A. Kumar, F. Avecillac, J. C. Pessoa, *Dalton Trans.* **2009**, (43), 9555.

[30] M. R. Maurya, N. Chaudhary, F. Avecilla, I. Correia, *J. Inorg. Biochem.* **2015**, *147*, 181.

[31] Z. R. Tshentu, C. Togo, R. S. Walmsley, *J. Mol. Catal. A Chem.* **2010**, *318*, 30.

[32] A. S. Ogunlaja, W. Chidawanyika, E. Antunes, M. A. Fernandes, T. Nyokong, N. Torto, Z. R. Tshentu, *Dalton Trans.* **2012**, *41*, 13 908.

[33] R. S. Walmsley, A. S. Ogunlaja, M. J. Coombes, W. Chidawanyika, C. Litwinski, N. Torto, T. Nyokong, Z. R. Tshentu, *J. Mater. Chem.* **2012**, *22*, 5792.

[34] S. M. Islam, P. Mondal, K. Tuhina, A. S. Roy, D. Hossain, S. Mondal, *Transition Met. Chem.* **2010**, *35*, 891.

[35] M. R. Maurya, A. Arya, P. Ada, J. C. Pessoa, *Appl. Catal. A* **2008**, *351*, 239.

[36] M. R. Maurya, M. Kumar, A. Kumar, J. C. Pessoa, *Dalton Trans.* **2008**, (32), 4220.

[37] K. Kamata, R. Ishimoto, T. Hirano, S. Kuzuya, K. Uehara, N. Mizuno, *Inorg. Chem.* **2010**, *49*, 2471.

[38] M. R. Maurya, P. Saini, C. Haldar, A. K. Chandrakar, S. Chand, *J. Coord. Chem.* **2012**, *65*, 2903.

[39] J. Tong, W. Li, L. Bo, H. Wang, Y. Hu, Z. Zhang, A. Mahboob, *J. Catal.* **2016**, *344*, 474.

[40] (a)G. Yang, M. D. Huff, H. Du, Z. Zhang, Y. Lei, *Cat. Com.* **2017**, *99*, 43. (b)S. Balasubramanyan, S. Arayathody, S. Sugunan, *Mater. Chem. Phys.* **2018**, *211*, 23. (c)M. Kohantorabi, M. R. Gholami, *Mater. Chem. Phys.* **2018**, *213*, 472. (d)X. Feng, J. Hao, Y. Gao, W. Bai, Y. Cheng, F. Wang, L. Han, Q. Suo, Y. Wang, *Cat. Com.* **2018**, *104*, 48. (e)W. Zhong, M. Liu, J. Dai, J. Yang, L. Mao, D. Yin, *Appl. Catal. Environ.* **2018**, *225*, 180. (f)Y. Hakat, T. V. Kotbagi, M. G. Bakker, *J. Mol. Catal. A Chem.*

2016, *411*, 61. (g)F. P. da Silva, R. V. Gonçalves, L. M. Rossi, *J. Mol. Catal. A Chem.* **2017**, *426*, 534.

[41] G. Zhang, Y. Shi, Y. Wei, Q. Zhang, K. Cai, *Inorg. Chem. Commun.* **2017**, *86*, 112.

[42] X. Hou, Z. Wang, C. Fang, T. Li, S. Pan, *Appl. Surf. Sci.* **2018**, *455*, 561.

[43] G. Zhang, Y. Shi, Y. Wei, Q. Zhang, Y. Zhang, K. Cai, S. Xiu, *Inorg. Chem. Commun.* **2018**, *91*, 81.

[44] A. Patel, R. Sadasivan, *Inorg. Chim. Acta* **2017**, *458*, 101.

[45] C. A. Deshmane, J. B. Jasinski, P. Ratnasamy, M. A. Carreon, *Cat. Com.* **2011**, *15*, 46.

[46] M. Bonchio, M. Carraro, A. Farinazzo, A. Sartorel, G. Scorrano, U. Kortz, *J. Mol. Catal. A Chem.* **2007**, *262*, 36.

[47] K. B. Vu, T. K. Phung, *J. Ind. Eng. Chem.* **2016**, *40*, 40.

[48] T. Joseph, D. Srinivas, C. S. Gopinath, S. B. Halligudi, *Catal. Lett.* **2002**, *83*, 209.

[49] A. Zsigmond, A. Horvath, F. Notheisz, *J. Mol. Catal. A Chem.* **2001**, *171*, 95.

[50] V. Hulea, E. Dumitriu, *Appl. Catal. Gen.* **2004**, *277*, 99.

[51] A. S. Sharma, H. Kaur, *Appl. Catal. A* **2017**, *546*, 136.

[52] N. C. Desai, J. A. Chudasama, T. J. Karkar, B. Y. Patel, K. A. Jadeja, D. R. Godhani, J. P. Mehta, *J. Mol. Catal. A Chem.* **2016**, *424*, 203.

[53] Y. Long, Z. Zhao, L. Wu, S. Luo, H. Wen, W. Wu, H. Zhang, J. Ma, *Mol. Catal.* **2017**, *433*, 291.

[54] J. H. Noh, R. Patala, R. Meijboom, *Appl. Catal. A* **2016**, *514*, 253.

[55] (a)C. L. Marchena, G. A. Pecchi, L. B. Pierella, *Cat. Com.* **2019**, *119*, 28. (b)B. Sakthivel, D. Santhakumar, R. Josephine, K. Sethuraman, A. Dhakshinamoorthy, *Cat. Com.* **2018**, *108*, 41. (c)Y. X. Li, Z. Y. Wei, L. Liu, M. L. Gao, Z. Bo Han, *Inorg. Chem. Commun.* **2018**, *88*, 47. (d)N. Masunga, G. S. Tito, R. Meijboom, *Appl. Catal. A* **2018**, *552*, 154. (e)N. Masunga, B. P. Doyle, E. Carleschi, R. Meijboom, *Appl. Catal. A* **2018**, *559*, 175. (f)Y. H. Fu, L. Xu, H. M. Shen, H. Yang, F. M. Zhang, W. D. Zhu, M. H. Fan, *Chem. Eng. J.* **2016**, *299*, 135. (g)D. M. Gao, Q. M. Gao, *Cat. Com.* **2007**, *8*, 681. (h)Y. Wu, Y. Zhang, J. Cheng, Z. Li, H. Wang, Q. Sun, B. Han, Y. Kong, *Micropor. Mesopor. Mater.* **2012**, *162*, 51. (i)W. L. Sun, J. L. Hu, *React. Kinet. Mech. Cat.* **2016**, *119*, 305. (j)J. H. Tong, X. D. Cai, H. Y. Wang, Q. P. Zhang, *Mater. Res. Bull.* **2014**, *55*, 205. (k)V. Hulea, E. Dumitriu, *Appl. Catal. A* **2004**, *277*, 99.

[56] Y. Yoshimura, Y. Ogasawara, K. Suzuki, K. Yamaguchi, N. Mizuno, *Cat. Sci. Technol.* **2017**, *7*, 1662.

[57] A. Rezaeifard, M. Jafarpour, R. Haddad, F. Feizpour, *Cat. Com.* **2017**, *95*, 88.

[58] P. J. Baricelli, V. J. Sanchez, A. J. Pardey, S. A. Moya, *J. Mol. Catal. A* **2000**, *164*, 77.

[59] H. Li, B. Xu, B. Deng, X. Yan, Y. Zheng, *Cat. Com.* **2014**, *46*, 224.

[60] S. J. Bora, R. Paul, M. Nandi, P. K. Bhattacharyya, *J. Solid State Chem.* **2017**, *256*, 38.

[61] P. Tau, T. Nyokong, *J. Mol. Catal. A Chem.* **2007**, *273*, 149.

[62] X. Song, W. Z. Y. Yan, H. Gao, W. Gao, *J. Mol. Catal. A Chem.* **2016**, *413*, 32.

[63] Q. N. Zhang, J. Zhang, T. H. Wu, X. P. Zhou, *Cat. Com.* **2009**, *10*, 1279.

[64] U. R. Pillai, E. S. Demessie, R. S. Varma, *Tetrahedron Lett.* **2002**, *43*, 2909.

[65] V. Conte, A. Coletti, B. Floris, G. Licini, C. Zonta, *Coord. Chem. Rev.* **2011**, *255*, 2165.

[66] J. A. L. d. Silva, J. J. R. F. da Silva, A. J. L. Pombeiro, *Coord. Chem. Rev.* **2011**, *255*, 2232.

[67] H. Mimoun, I. Seree de Roch, L. Sajus, *Tetrahedron* **1970**, *26*, 37.

[68] P. Chaumette, H. Mimoun, L. Saussine, J. Fischer, A. Mitschler, *J. Organomet. Chem.* **1983**, *250*, 291.

[69] K. B. Sharpless, J. M. Townsend, D. R. Williams, *J. Am. Chem. Soc.* **1972**, *94*, 295.

[70] M. R. Maurya, C. Haldar, S. Behl, N. B. Kamatham, F. Avecilla, *J. Coord. Chem.* **2011**, *64*(17), 2995.

[71] (a)S. Huber, M. Cokoja, F. E. Kühn, *J. Organomet. Chem.* **2014**, *751*, 25. (b)P. Gisdakis, V. Yudanov, N. Rösch, *Inorg. Chem.* **2001**, *40*, 3755. (c)D. V. Deubel, J. Sundermeyer, G. Frenking, *J. Am. Chem. Soc.* **2000**, *122*, 10 101. (d)D. V. Deubel, G. Frenking, P. Gisdakis, W. A. Herrmann, N. Rösch, J. Sundermeyer, *Acc. Chem. Res.* **2004**, *37*, 645.

[72] E. I. Solomon, P. Chen, M. Metz, S. K. Lee, A. E. Palner, *Angew. Chem. Int. Ed.* **2001**, *40*, 4570.

[73] J. P. Klinman, *Chem. Rev.* **1996**, *96*, 2541.

[74] S. Mukherjee, S. Samanta, A. Bhaumik, B. C. Ray, *Appl. Catal. B* **2006**, *68*, 12.

SUPPORTING INFORMATION

Additional supporting information may be found online in the Supporting Information section at the end of the article.

How to cite this article: Maurya A, Kesharwani N, Kachhap P, Mishra VK, Chaudhary N, Haldar C. Polymer-anchored mononuclear and binuclear Cu^{II} Schiff-base complexes: Impact of heterogenization on liquid phase catalytic oxidation of a series of alkenes. *Appl Organometal Chem*. 2019;e5094; e5094. https://doi.org/10.1002/aoc.5094